FINAL REPORT FOR PROJECT FUNDING FROM USGS

1. administrative

Principal Investigator:	Ming Xue (mxue@ou.edu) (405) 325-0453 Fax: (405) 325-7614	**Institution:**	University of Oklahoma
Project title:	Informing Hydrologic Planning in the Red River Valley through Improved Regional Climate Projections		
Agreement number:	G15AP00131	**Date of report:**	Feb, 2018
Period of time covered by the report	09/25/15- 09/25/17		
Actual total cost			

2. public summary

The U.S. Great Plains is known for frequent hazardous convective weather and climate extremes. Across this region, climate change is expected to cause more severe droughts, more intense heavy rainfall events, and subsequently more flooding episodes. These potential changes in climate will adversely affect habitats, ecosystems, and landscapes as well as the fish and wildlife they support. Better understanding and simulation of regional precipitation can help natural resource managers mitigate and adapt to these adverse impacts.

In this project, we aim to achieve a better precipitation downscaling in the Great Plains with the Weather Research and Forecast (WRF) model and use the high quality dynamic downscaling results (with a 4km horizontal resolution) to investigate the precipitation variability near the Edwards Plateau and Balcones Escarpment in Texas, an area prone to heavy rain and devastating flood events.

To this end, WRF simulations with different physics schemes and nudging strategies are first conducted for a representative warm season. Results show that simply choosing different physics schemes is not enough to alleviate the dry bias over the southern Great Plains, which is related to an anticyclonic circulation anomaly over the central and western parts of continental

U.S. in the simulations. Spectral nudging emerges as an effective solution for alleviating the precipitation bias. As a result, a better precipitation downscaling is achieved. With the carefully designed configurations, WRF downscaling is conducted for 1980-2015. The downscaling captures well the spatial distribution of monthly climatology precipitation and the monthly/yearly variability, showing improvement over at least two previously published precipitation downscaling studies. With the improved precipitation downscaling, a better hydrological simulation over the trans-state Oologah watershed is also achieved. In addition, analyzing the high-resolution (4 km) downscaling outputs leads to a better understanding regarding the precipitation variability in Texas.

3. technical summary

Detailed, regional climate projections, particularly for precipitation, are critical for many applications, including hydrologic assessment. Accurate precipitation downscaling in the United States Great Plains remains a great challenge for most Regional Climate Models, particularly for warm months. Most previous dynamic downscaling simulations significantly underestimate warm-season precipitation in the region.

This study aims to first achieve a better precipitation downscaling in the Great Plains with the Weather Research and Forecast (WRF) model. To this end, WRF simulations with different physics schemes and nudging strategies are first conducted for a representative warm season. Results show that different cumulus schemes lead to more pronounced difference in simulated precipitation than other tested physics schemes. Simply choosing different physics schemes is not enough to alleviate the dry bias over the southern Great Plains, which is related to an anticyclonic circulation anomaly over the central and western parts of continental U.S. in the simulations. Spectral nudging emerges as an effective solution for alleviating the precipitation bias. Spectral nudging ensures that large and synoptic-scale circulations are faithfully reproduced while still allowing WRF to develop small-scale dynamics, thus effectively suppressing the large-scale circulation anomaly in the downscaling. As a result, a better precipitation downscaling is achieved. With the carefully validated configurations, WRF downscaling is conducted for 1980-2015. The downscaling captures well the spatial distribution of monthly climatology precipitation and the monthly/yearly variability, showing improvement over at least two previously published precipitation downscaling studies. With the improved

precipitation downscaling, a better hydrological simulation over the trans-state Oologah watershed is also achieved.

In addition, high resolution (4km) dynamic downscaling results were used to investigate the precipitation variability near the Edwards Plateau and Balcones Escarpment in Texas, an area prone to heavy rain and devastating flood events. Analysis results indicate that the total August precipitation east of the Balcones Escarpment is suppressed and precipitation over the eastern part of the Edwards Plateau is enhanced. Locally initiated moist convection in the afternoon contributes most to the total precipitation during August in the region. The dynamic downscaling output captures the spatial pattern of afternoon precipitation, which is well aligned with the simulated upward motions. The clay-based soil types that dominate the Edwards Plateau have great potential to retain soil moisture and limit latent heat fluxes, consequently leading to higher sensible heat flux than over the plain to the east. As a result, vertical motion is induced, triggering the afternoon moist convection over the Edwards Plateau under favorable conditions. In comparison, the sloping terrain plays a smaller role in triggering the convection.

4. purpose and objectives

Across the Southern Great Plains, climate change is expected to cause more severe droughts, more intense heavy rainfall events, and subsequently more flooding episodes. These potential changes in climate will adversely affect habitats, ecosystems, and landscapes as well as the fish and wildlife they support. Better projections of regional precipitation and hydrological response in future climates will help mitigate these adverse impacts. Warm-season convective precipitation is a major driver of the hydrological cycle across the Plains, but convection is very difficult to predict accurately, especially when using today's global climate models (GCMs) whose typical grid cells (50 to 100 km) are larger than the sizes of convective storms. To explicitly resolve convection, a horizontal grid spacing of 4 km or less is needed. As a result, the projection of precipitation and hydrological cycles based on GCMs tend to be unreliable.

Given these challenges, this project (**Informing Hydrologic Planning in the Red River Valley through Improved Regional Climate Projections**) addressed the over-arching theme of the South-Central Climate Science Center (SC-CSC) solicitation, "Precipitation Variability" within the region, by: (i) establishing high-resolution regional climate dynamic downscaling capabilities that can more accurately simulate precipitation-related variability and trends, (ii) applying these

climate downscaling for long-term hydrological planning for the South-Central region. By using a convection-permitting resolution, precipitation and its hydrological response can be much more accurately simulated, which is critical for more accurately quantifying the impacts of climate change on agriculture, fish and wildlife, water availability and quality, all of which are key challenges facing the Landscape Conservation Cooperatives (LCCs) of the region.

5. approach

a) Precipitation observations

The Stage IV precipitation data [*Lin*, 2011] have been archived continuously since January 2002, and they are available via http://data.eol.ucar.edu/codiac/dss/id=21.093. The precipitation data have a consistent analysis record length of 15 years, and have high temporal and spatial resolutions that are valuable to this study [*Herman and Schumacher*, 2016]. The Stage IV data combine the mosaicked hourly/6-hourly multi-sensor (i.e., radars and gauges) precipitation analyses (called Stage III) produced by the 12 River Forecast Centers of the National Weather Service. The data cover the contiguous United States (CONUS) and have a grid spacing of 4 km. The products are available for hourly, 6-hourly, and daily intervals. Stage IV data display an overall agreement with surface observations, although the products have a tendency to underestimate both annual and seasonal means as compared to surface observations [*Nelson et al.*, 2016].

To make up the deficiency of relatively short record (15 years) of the Stage IV data, the Parameter-elevation Regressions on Independent Slopes Model (PRISM) precipitation dataset [*Daly et al.*, 1994] is selected for a longer-term model evaluation. PRISM produces monthly and annual average precipitation since 1895 (downloaded from http://www.prism.oregonstate.edu/) on regularly spaced grid cells over the CONUS domain at various spatial resolutions (800 m to 4 km) based on point measurements and a digital elevation model [*Prat and Nelson*, 2015]. We use the 4-km resolution monthly PRISM precipitation data in this study. Stage IV and PRISM data show similar spatial distributions of precipitation.

b) Study Periods

Our previous study [*X Sun et al.*, 2016] and the NARCCAP regional climate simulations [*Mearns et al.*, 2012] significantly underestimate warm-season precipitation over the Great Plains, corroborating the generally accepted conclusion that accurate downscaling of summer precipitation in this region remains a great challenge for most RCMs [*Liang et al.*, 2006; *F X Qiao and Liang*, 2015; *J L Wang and Kotamarthi*, 2014]. Thus, to attain our goal of improving precipitation simulations over the Great Plains,

we first focus on a single summer season (June, July, and August, i.e., JJA). We chose summer 2005 because it had sufficient rainfall to compare with simulations; in fact, the summer of 2005 was much wetter over the Great Plains than spring or fall of 2005 [*Ramsey et al.*, 2014]. A band of maximum precipitation over the Great Plains in JJA 2005 extended from north Texas northward to Kansas, where it peaked. Previous downscaling for this period conducted by *J L Wang and Kotamarthi* [2014] also shows significant dry bias over the Great Plains.

To investigate the possible model errors responsible for the bias in downscaled precipitation, we conduct a nearly exhaustive set of sensitivity experiments for the month of August 2005 using different combinations of physics parameterization schemes available within WRF. After we have identified the model configuration with the least precipitation bias for the Great Plains, we use it to dynamically downscale the NCEP/DOE R2 data [*Kanamitsu et al.*, 2002; *National Centers for Environmental Prediction National Weather Service Noaa U. S. Department of Commerce*, 2000] for a 36-year period (1980-2015). This period is selected to encompass the 25-year time span (1980-2004) of the NARCCAP experiments as well as more recent years. In these multi-year downscaling simulations, the model is reinitialized every year following the approach of *J L Wang and Kotamarthi* [2014], but allowing for one extra month of spin-up, i.e., the model starts from 1 December of the previous year, runs for 13 months, and the outputs of the last 12 months are used for analysis. This reinitialization procedure allows for parallel executions of simulations for different years, improving the overall computational efficiency and turn around time on large parallel computers. We have compared results of reinitialized simulations with simulations continued from the end of the previous year; the differences are minimal as long as the spectral nudging is turned on because of the apparent lack of the initial condition memory beyond one month, in these simulations that are primarily forced at the lateral boundaries and interiorly nudged to the reanalysis data for long waves.

c) Three-dimensional WRF simulations

The WRF model has been used in a number of regional climate studies at various horizontal resolutions, including 12 to 50 km grid spacings [*Bukovsky and Karoly*, 2009; *Leung et al.*, 2006; *Lo et al.*, 2008; *J L Wang and Kotamarthi*, 2014; *Wi et al.*, 2012; *Y X Zhang et al.*, 2009]. Recently, it has been applied at the convection-permitting, 4-km grid spacing over large regions [*Y Gao et al.*, 2012; *H Lee et al.*, 2017; *Andreas F. Prein et al.*, 2017; *X Sun et al.*, 2016]. However, such long-term, high-resolution simulations over large domains are computational very expensive and are not necessarily free of biases [*F X Qiao and Liang*, 2015; *X Sun et al.*, 2016]; in fact, the 4-km WRF simulations reported in Sun et al. (2016) share similar precipitation biases as coarser resolution simulations that we have produced (not shown). For these reasons, we apply in this study WRF version 3.8.1 at a 20-km grid spacing and use it to downscale from the NCEP/DOE R2 data over the CONUS domain (see Fig. 1b). The model domain has

44 vertical layers extending from the surface to 100 hPa. The control configuration for WRF includes the Dudhia shortwave radiation scheme [*Dudhia*, 1989], the rapid radiative transfer model (RRTM) [*Mlawer et al.*, 1997] for longwave radiation, the Noah land surface model [*Chen and Dudhia*, 2001], the Yonsei University (YSU) boundary layer scheme [*S Y Hong et al.*, 2006], the Grell-Freitas cumulus scheme [*Grell and Freitas*, 2014], and the Morrison microphysics scheme [*Morrison et al.*, 2009]. No interior nudging is applied in the control configuration.

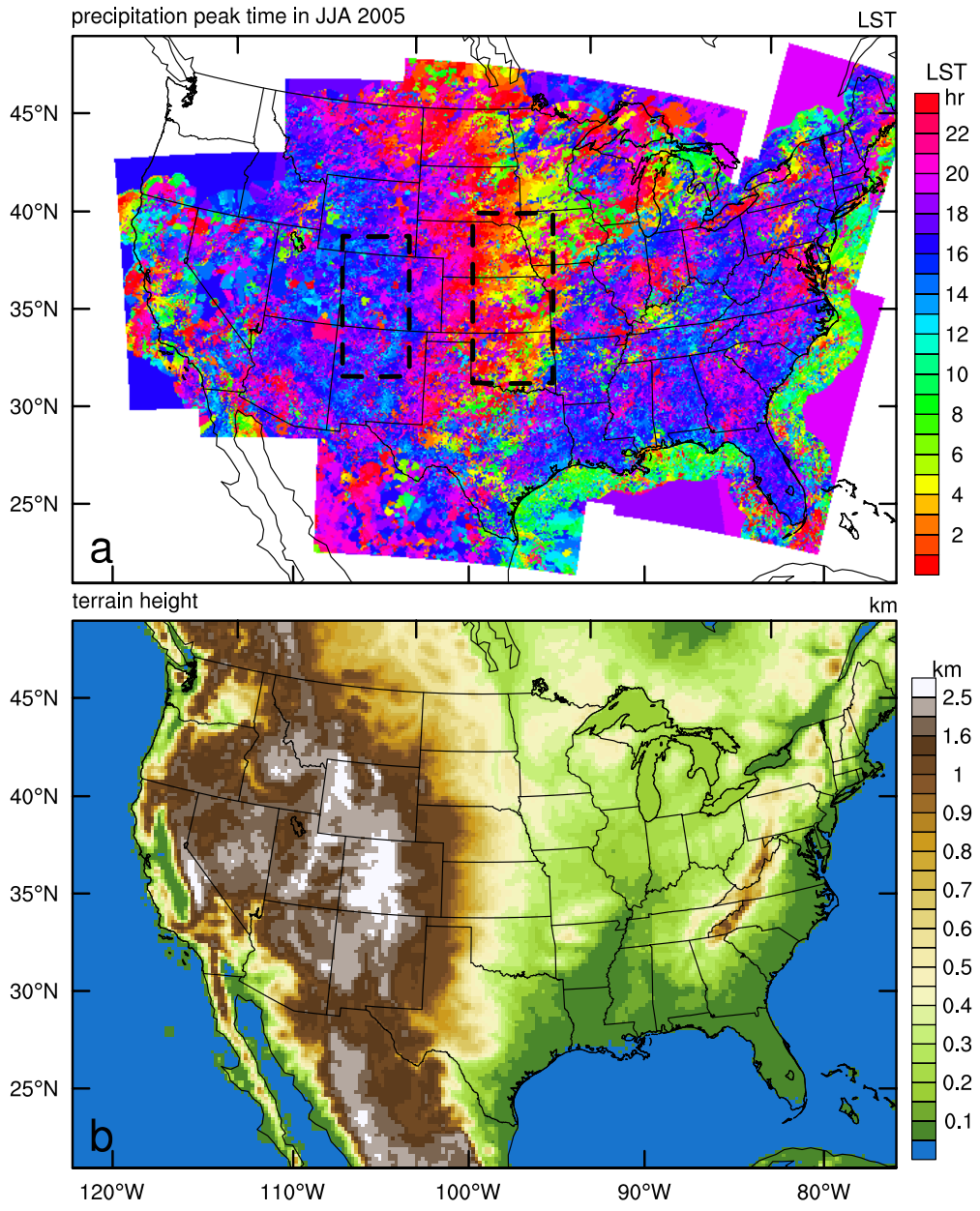

Fig. 1. (a) Precipitation peak time (in Local Standard Time, LST) in JJA 2005 calculated from the Stage IV precipitation data and (b) terrain height in the WRF modeling domain. The two rectangular boxes in panel (a) marks the areas of Rockies and Great Plains over where the diurnal variation of precipitation is examined and statistics of simulated precipitation are calculated.

Based on the control simulation, we conduct sensitivity experiments with 9 cumulus, 20 microphysics, 2 land surface, and 7 boundary-layer schemes (total 9+20+2+7=38 experiments) for summer 2005. These physics parameterization schemes have been shown to markedly affect downscaled precipitation output in previous studies [*C Klein et al.*, 2015]. The full list and description of the parameterization schemes can be found at http://www2.mmm.ucar.edu/wrf/users/docs/user_guide_V3.8/users_guide_chap5.htm#summary. To ensure that the forcing data does not affect our results significantly, we also conduct sensitivity simulations for summer 2005 using two other reanalysis data sets, i.e., the North American Regional Reanalysis (NARR) [*Mesinger et al.*, 2006; *National Centers for Environmental Prediction National Weather Service Noaa U. S. Department of Commerce*, 2005] and the ERA-interim data [*European Centre for Medium-Range Weather Forecasts*, 2009]. Most importantly, we examine the impact of applying interior spectral nudging through experiments with and without the nudging.

d) Hydrologic simulations with the VIC model

Using simulations with the VIC model, *L Qiao et al.* [2014b] assessed the hydrological responses of the trans-state Oologah Lake watershed in the Great Plains to the historical and future downscaled output from NARCCAP. The Oologah Lake watershed covers a typical tallgrass prairie with dominant land use of rangelands and farming lands extending from southeast Kansas to northeast Oklahoma in the southern Great Plains. Warm season convective precipitation is a very important part of water inputs to the watershed. Intervening flood and drought hazards are very common in the watershed due to the highly dynamic weather, which would be intensified in a changing climate. Thus, improved climate projection and better assessment of hydrological response of this watershed is highly warranted for effective hazard mitigation, natural resource management and climate change adaptation [*L Qiao et al.*, 2017; *L Qiao et al.*, 2014a]. For these reasons, we conduct hydrological simulations using VIC model to assess the hydrological responses of the Oologah Lake watershed (particularly in terms of streamflow amplitudes) to the WRF-downscaled precipitation obtained in this study and to the NARCCAP WRFG-downscaled precipitation. The VIC-simulated streamflow rates at the watershed outlet (the Verdigris River near Lenapah, Oklahoma) were initially calibrated and

validated at daily time scale using atmospheric forcing from the University of Washington's gridded dataset [*Maurer et al.*, 2002]. This dataset is similar to the PRISM dataset with the elevation effect considered. The streamflow dataset is downloaded from the United States Geological Survey (USGS) water information website (http://waterdata.usgs.gov/nwis). The VIC model, calibrated with the automatic procedure of SP-UCI (Shuffled complex with Principle component analysis) [*Chu et al.*, 2011], simulates the observed streamflow in a high degree of agreement with NSCE (Nash-Sutcliffe Efficiency) of 0.74 and 0.8 respectively for 1990-1997 (calibration) and 1968-1989 (validation). More detailed configuration and performance of the VIC model simulations can be seen in *L Qiao et al.* [2014b].

6. project results

6.1. Improvement of precipitation downscaling in summer 2005

Our previous 10-year dynamic downscaling significantly underestimates warm-season precipitation over the Great Plains [*X Sun et al.*, 2016]. The same issue also occurs with NARCCAP 25-year downscaling, particularly with the WRFG member [*Mearns et al.*, 2012]. To diagnose the issue, we first perform WRF simulations using NCEP/DOE R2 for JJA 2005. Similar to Sun et al. (2016), the WRF model with the control configuration again significantly underestimates the precipitation over the Great Plain area (by -49.7%), especially over Kansas and Oklahoma (Fig. 2c), even though the configuration of this study is different from that used in Sun et al. (2016). Results for the single month of August 2005 (Fig. 3b) are similar to that of JJA. Because regional WRF simulations have been shown to be sensitive to the uncertainties in the large-scale forcing [*Michelson and Bao*, 2008], we also used two other reanalysis data sets (i.e., ERA-interim, and NARR) to drive the WRF downscaling. Although sensitivities of the downscaling results to the reanalysis data sets are found, the spatial distribution of the downscaled precipitation is not improved with the use of different reanalysis forcing (Fig. 2). With NARR, the Great Plains appear even drier (underestimated by -52%), with the precipitation over Nebraska significantly reduced. These simulations indicate that the dry bias over the Great Plains seen in previous studies is not caused by a particular reanalysis product. In addition, a similar dry bias in the Great Plains has also been reported from simulations using other regional climate models [*Berg et al.*, 2013; *Harris and Lin*, 2014; *M I Lee et al.*, 2007b; *Ma et al.*, 2014] and speculated to be related to unrealistically strong coupling of convective processes to the surface heating over the Rocky Mountains and to abnormally slow eastward propagation of convective systems [*S A Klein et al.*, 2006; *M I Lee et al.*, 2007b; *Tripathi and Dominguez*, 2013].

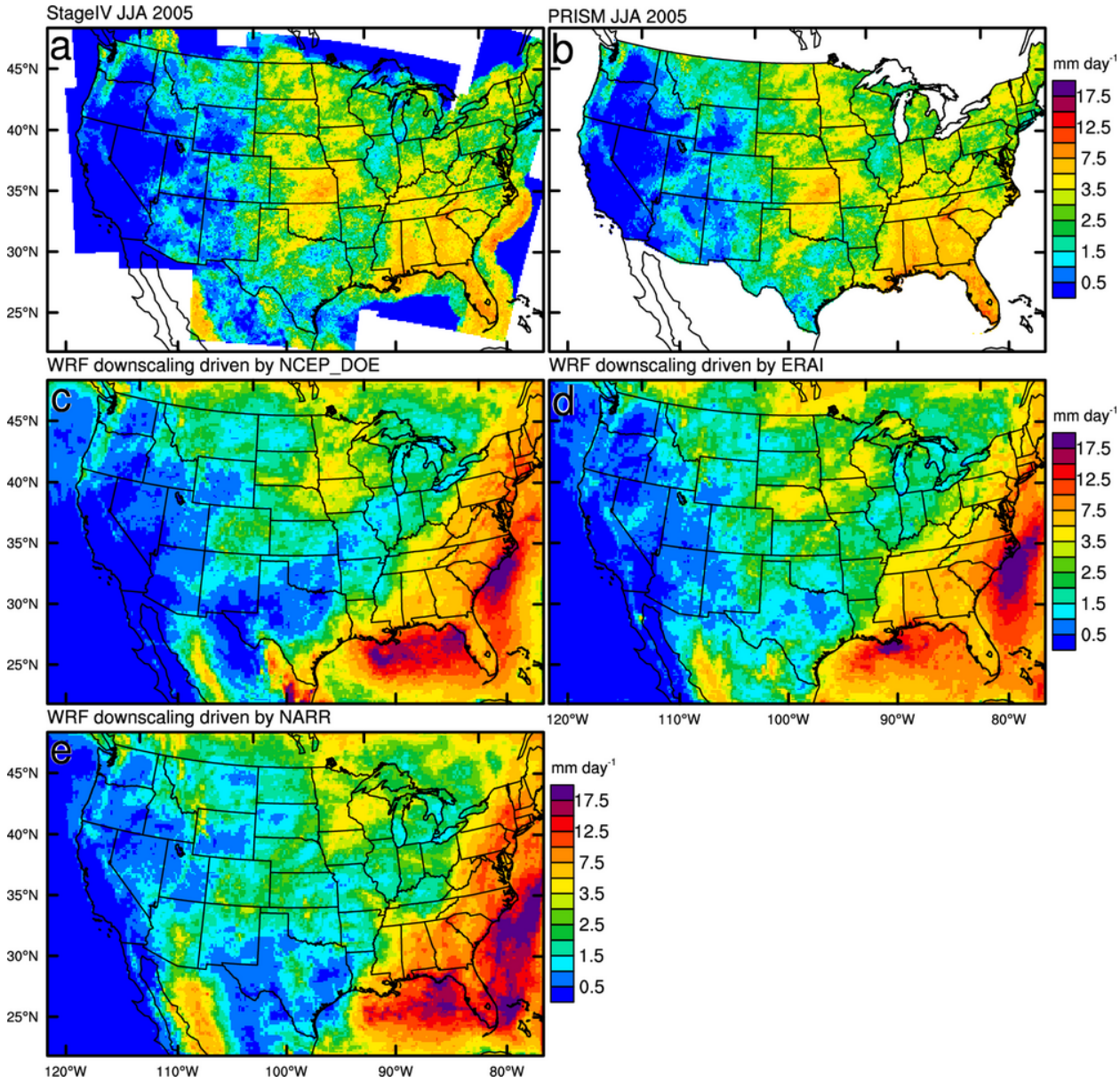

Fig. 2. Mean precipitation rate in JJA 2005 retrieved from (a) StageIV, (b) PRISM data, and dynamically downscaled with WRF from the (c) NCEP/DOE R2, (d) ERA-interim, and (e) NARR reanalysis data.

To investigate if certain model physics parameterizations can alleviate the warm-season dry bias over the Great Plains, we ran a large set of sensitivity simulations with 9 cumulus schemes, 2 land surface models, 7 PBL schemes, and 20 microphysics schemes for a representative month (i.e., August 2005) when WRF simulations suffer severe dry bias over the southern Great Plains. Unfortunately, all of these simulations show similar biases in terms of precipitation location (results from 3 sensitivity simulations are shown in Fig. 3b-d); that is, precipitation in Kansas, Oklahoma, and Texas is underestimated (similar as the JJA mean shown in Fig. 2) and precipitation in the Rockies is overestimated, thus shifting the southern Great Plains rain band northwestward, as is also reported in Sun et al. (2016) (see their Fig. 2).

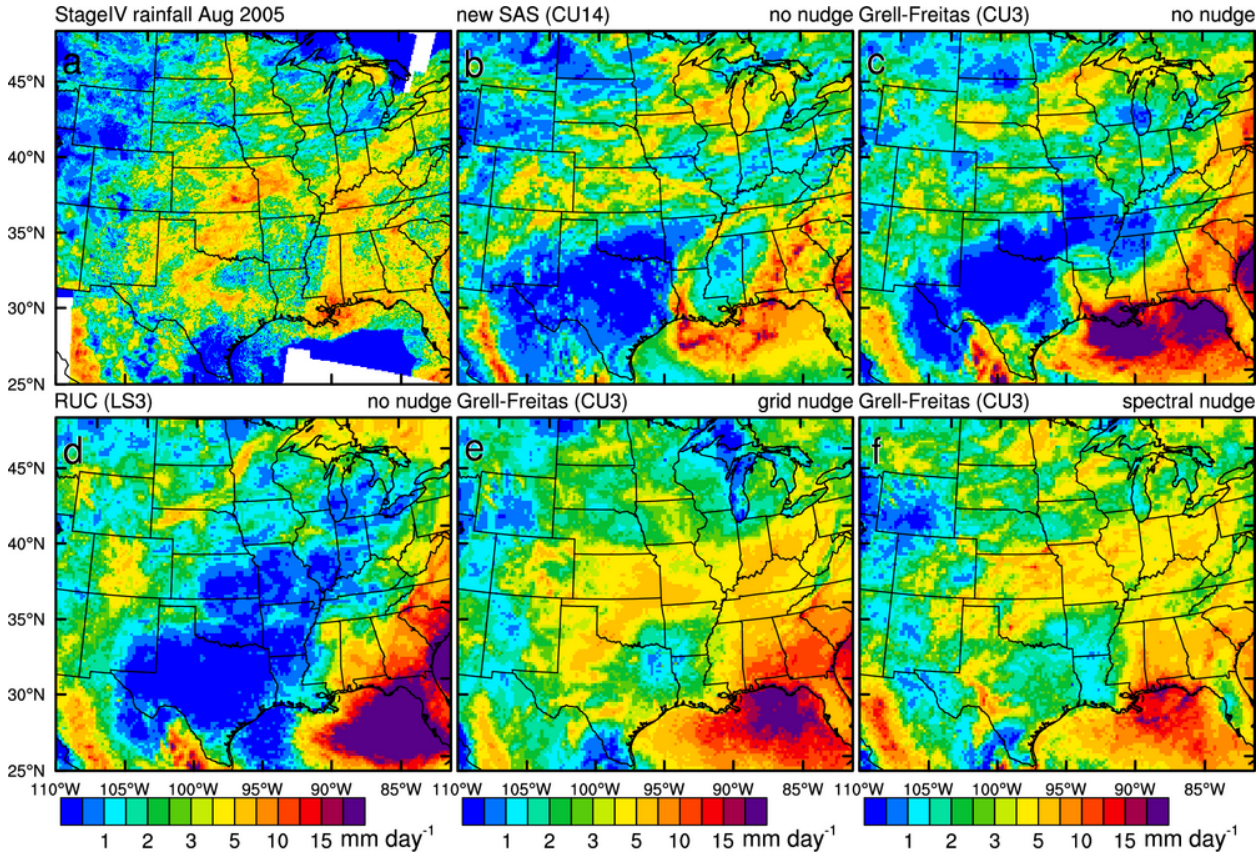

Fig. 3. Mean precipitation rate in August 2005 retrieved from (a) the StageIV data and dynamically downscaled with WRF (b,c,d) with different physics schemes but no nudging, (e) with grid nudging, and (f) with spectral nudging.

Over the past several years, the Center for Analysis and Prediction of Storms at the University of Oklahoma has been carrying out real-time numerical weather prediction (NWP) using the WRF model, with a focus on precipitation and severe weather [*Kong et al.*, 2011; *Xue et al.*, 2007; *Xue et al.*, 2009; *Xue et al.*, 2010]. In these real-time forecasts up to several days, systematic bias in precipitation location around the Great Plains does not occur. Thus, we suspect that the bias in the regional climate simulations is rooted in the downscaling framework. The core differences between NWP and climate downscaling include: (1) different driving data (i.e., forecast data for NWP versus reanalysis data for downscaling of the historical period); and (2) different initialization strategies (i.e., daily reinitialization for short-term NWP versus a single initialization for continuous, long-range simulations). However, reanalysis data should be generally more accurate than the forecast data used at the lateral boundaries because of all the observations assimilated into the reanalysis fields. In addition, our simulations driven by different reanalysis datasets (Fig. 2) share similar precipitation biases. Thus, it is unlikely that systematic biases in the driving reanalysis data caused the precipitation biases.

Given the above discussions, we speculate that error accumulation within the long regional climate simulations as an important cause for the systematic precipitation bias. To assess this speculation,

instead of initializing once and running the simulation for a full month of August, we reinitialize the simulations on a daily basis (similar to the NWP runs). When the simulations are reinitialized daily, the southern Great Plains rain band is indeed much better reproduced, particularly in terms of its location (figure not shown). The sensitivity to the initialization strategies indicates that model bias accumulated through the continuous (monthly, seasonally, or longer) climate simulations does appear to be a key reason for the simulated precipitation biases. For regional climate simulations, daily reinitialization from reanalysis is clearly not an acceptable strategy. Ideally, the true source of model error causing the error accumulation is uncovered and an improvement to the model is implemented to reduce the error. Unfortunately, our exhaustive testing with different combination of model physics parameterizations did not give us much of a clue; finding a fix to the simulation model has to be left for further studies.

In the absence of a true fix to the model bias, one possible solution to prevent the systematic solution drift is to nudge the large-scale fields within the simulation domain towards the external forcing. Interior nudging had proven successful previously in dynamical downscaling of regional climate [*Hu et al.*, 2017; *Huang et al.*, 2016; *P Liu et al.*, 2012; *Lo et al.*, 2008; *Mabuchi et al.*, 2002; *Miguez-Macho et al.*, 2004; *Paul et al.*, 2016; *Andreas F. Prein et al.*, 2017; *Spero et al.*, 2014; *von Storch et al.*, 2000]. WRF supports two forms of interior nudging: analysis nudging (also called "grid nudging") and spectral nudging [*Miguez-Macho et al.*, 2004; 2005; *J L Wang and Kotamarthi*, 2013]. Analysis nudging adjusts simulations towards the driving fields (from the reanalysis or the GCM simulations) regardless of the scales of motion (thus also called indiscriminate nudging or non-scale-selective nudging) through adding a non-physical term to the model equation:

$$\frac{dQ}{dt} = L(Q) - K(Q - Q_o) \qquad (1)$$

where Q is any of the prognostic variables to be nudged, and Q_o is the corresponding variable from the driving fields, L is the model physical forcing term (including advection, Coriolis effects, etc.), K is the nudging coefficient, whose inverse is the e-folding time scale. In contrast, spectral nudging forces *only the long wavelengths* of nudged variables toward the driving fields [*Miguez-Macho et al.*, 2004] through

$$\frac{dQ}{dt} = L(Q) - \sum_{|n|\leq N} \sum_{|m|\leq M} K \cdot (Q_{mn} - Q_{omn}) e^{ik_m x} e^{ik_n y} \ , \qquad (2)$$

where m and n are number of waves in x and y directions, respectively, across the model domain, Q_{mn} and Q_{omn} are the spectral coefficients of Q and Q_o respectively. k_m and k_n are the wave vector components in the x and y directions, which are expressed in terms of discrete wave numbers m and n and domain size D_x and D_y :

$$k_m = \frac{2\pi \cdot m}{D_x};\ k_n = \frac{2\pi \cdot n}{D_y}\ . \tag{3}$$

Because the primary purpose of regional climate downscaling is to produce more smaller scale details not present in the driving large scale fields while trying to maintain a consistency between the downscale solutions and the driving fields at the large scales, spectral nudging is a reasonable choice for the downscaling purpose. Hence, we apply the spectral nudging configurations (including nudging variables, nudging strength, nudging height, wave number) suggested by *J L Wang and Kotamarthi* [2014] for their WRF-based downscaling. Particularly we adopted nudging wave numbers of 5 and 3 in the zonal and meridional directions over CONUS, thus nudging long waves with wavelengths of ~1000 km to those of the driving fields. The suggested nudging coefficient of 3×10^{-5} s^{-1} is adopted, which corresponds to a ~9 h time scale. Stronger nudging with larger nudging coefficients on more wave numbers was shown to have a detrimental effect on downscaled precipitation over the Great Plains, particularly on the detailed structures of precipitation, since it may destroy the mesoscale features simulated by the dynamic model [*Tian et al.*, 2017; *J L Wang and Kotamarthi*, 2014]. *Gomez and Miguez-Macho* [2017] explicitly suggest that 1000 km is the optimal scale threshold to nudge in order to balance the constrain from the driving fields and fine-scale contribution from the downscaling model.

Still, to examine the impacts of nudging over all wavenumbers, we also performed downscaling experiments with grid nudging. With either form of nudging, the simulated rain band location in the southern Great Plains during August 2005 is significantly improved (Fig. 3e-f). The model simulates more precipitation in Texas, Oklahoma, Kansas, and Missouri with either nudging than without, leading to a better agreement with the Stage IV data (Fig. 3a).

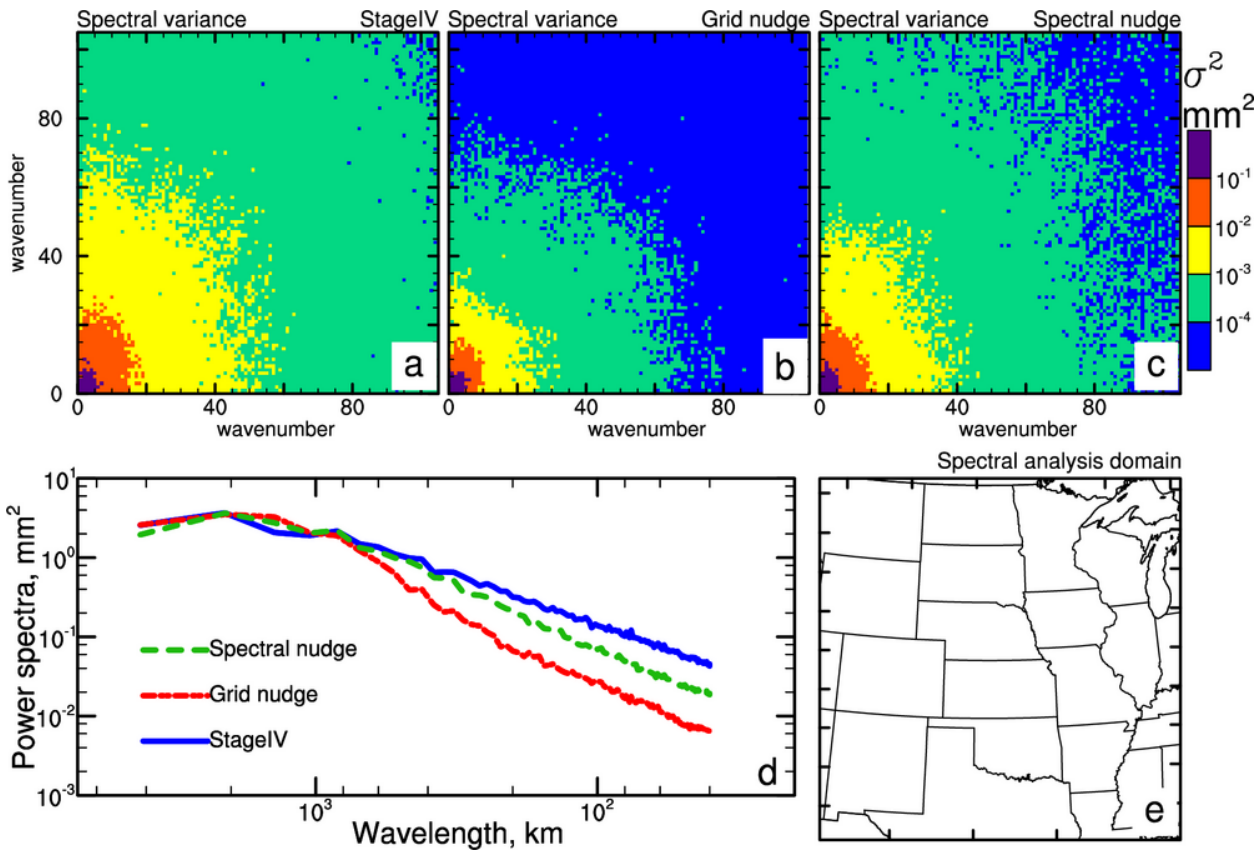

Fig. 4. Two-dimensional (2D) mean spectral variance of daily rainfall fields during August 2005 from (a) StageIV, (b) WRF downscaling with grid nudging, (c) WRF downscaling with spectral nudging computed using the discrete cosine transform (DCT) over the selected domain shown in panel (e). The 2D spectrum is binned according to equivalent wavenumbers to produce (d) the power spectra solely as a function of equivalent wavenumber (but not direction). Note that the StageIV has a higher resolution (~4km) than WRF (20km), thus can resolve more high frequency waves than WRF. But to compare with WRF, the larger wavenumbers resolved by StageIV are not shown in panels a and d.

Comparing to the spectral nudging, the grid nudging simulates wider spread precipitation with gentler spatial variations. A spectral analysis of the observed and downscaled precipitation fields using the Discrete Cosine Transform (DCT, *Denis et al.* [2002]) is conducted to further illustrate the difference in the effects of two forms of nudging. DCT is preferred over the Fourier transform for analyzing two-dimensional (2D) atmospheric fields over limited-area domains and it was previously used to evaluate precipitation forecasts [*Surcel et al.*, 2014]. 2D DCT spectral variance are computed for observed (i.e., StageIV) and downscaled daily precipitation fields during August 2005 within a square domain over the Great Plains. This square domain (Fig. 4e) is selected for three reasons: (1) precipitation variation over the Great Plains is the focus of this study, (2) the domain needs to be within the coverage of the StageIV data in order to compute the spectra of StageIV observations, (3) DCT analysis over a square domain is simpler and easier to interpret than that over a rectangle domain. The mean 2D spectral variance and the binned 1D power spectra during this month are shown in Fig. 4. Both grid nudging and spectral nudging

underestimate the variance of daily precipitation over short waves (with wavelength < 600 km) and the underestimation by grid nudging is more severe. The difference seen in Fig. 4 between grid nudging and spectral nudging can be explained by equations 1 and 2. Grid nudging adjusts nudged variables towards the driving fields (i.e., the R2 reanalysis) regardless of the scales of motions. Thus, the scale of motion resolved by the grid nudging is close to the R2 reanalysis (with a 2.5^{o} grid spacing), for which the smallest resolvable wavelength in DCT algorithm is ~500 km (2 grid spacing). Consequently, the smaller scale motion is damped during the grid nudging process. In contrast, spectral nudging only forces the long waves (with wavenumber ≤ 5 and 3 in zonal and meridional directions over the simulation domain, roughly wavelength >1000 km) of nudged variables to the driving fields and allow the model dynamics to develop small scale motions. Thus, the smallest resolvable wavelength in the DCT algorithm by the spectral nudging is 2 times model grid spacing, i.e., 40 km. As a result, the power spectra for short waves (<500 km) of nudged variables is less underestimated by spectral nudging than grid nudging, as also previously reported [e.g., *Gomez and Miguez-Macho*, 2017; *Otte et al.*, 2012; *Vincent and Hahmann*, 2015]. Precipitation, an un-nudged variable, responses to the nudged variables and also shows significant underestimation by grid nudging at scales with wavelength <500km (Fig. 4d). The spectral analysis thus further corroborates that spectral nudging is superior than grid nudging for dynamic downscaling.

Given the superiority over the downscaling without nudging or with grid nudging, spectral nudging is also applied in the downscaling of JJA 2005. Much better precipitation simulation is again obtained with spectral nudging for these months over the southern Great Plains (Fig. 5a) than without (Fig. 2c), as compared to the Stage IV dataset (Fig. 2a).

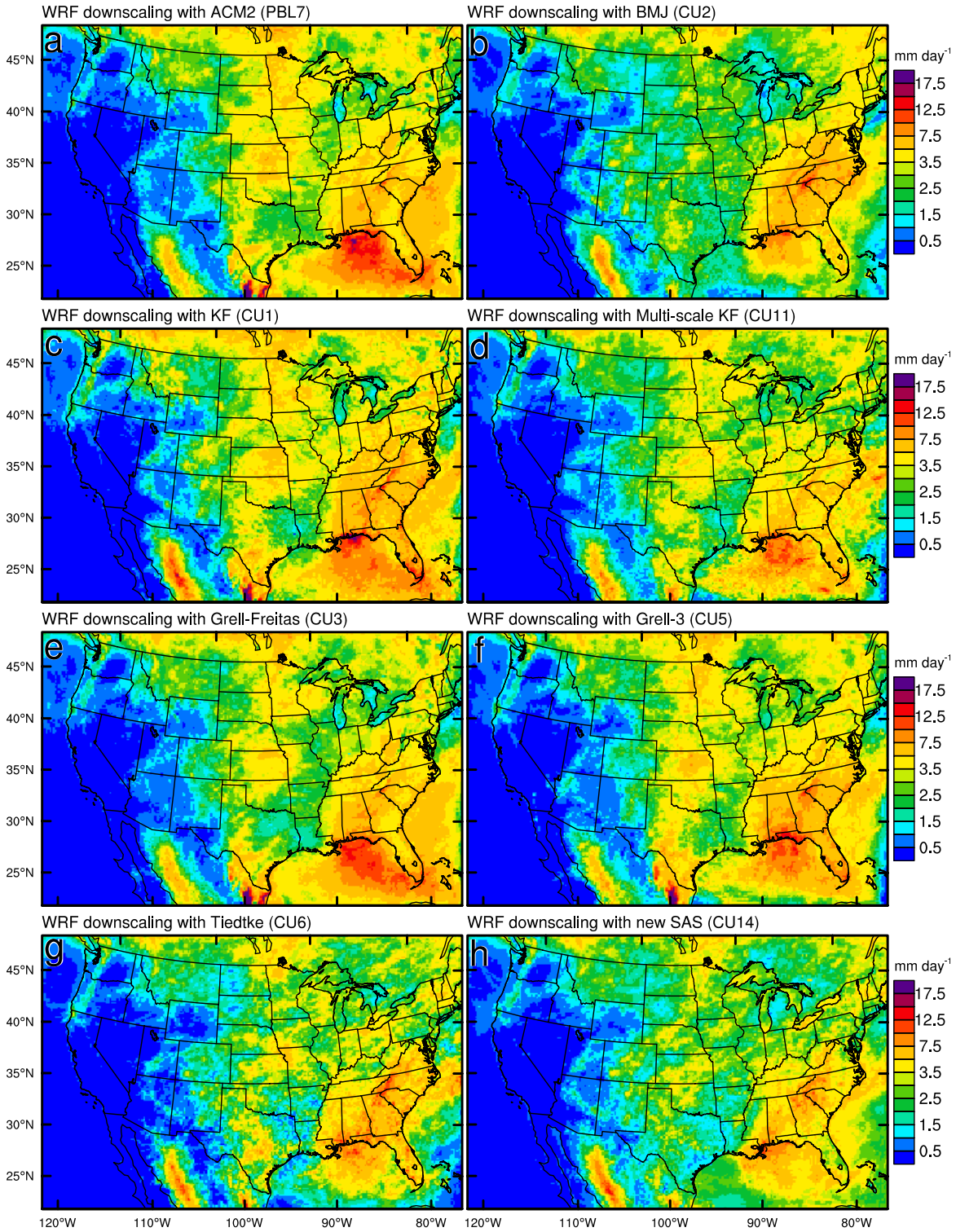

Fig. 5. Mean precipitation rate in JJA 2005 dynamically downscaled with WRF with spectral nudging and with (a) the ACM2 PBL scheme and with different cumulus schemes, i.e., (b) BMJ (CU2), (c) KF (CU1), (d) Multi-scale KF (CU11), (e) Grell-Freitas (CU3), (f) Grell-3 (CU5), (g) Tiedtke (CU6), (h) new SAS (CU14). The corresponding observations are shown in Fig. 2a,b.

The benefit of spectral nudging lies in its ability to constrain the large-scale circulation patterns in the regional domain to match those of external forcing. For example, Figure 6 shows the deviations of the simulated JJA mean circulation and geopotential height fields from those of NCEP R2 with and without spectral nudging. Relative to the driving NCEP R2 reanalysis, an anomalous anticyclonic circulation develops in the simulation without spectral nudging over the southern Great Plains and southwest U.S. while an anomalous cyclonic circulation occupies the eastern coastal region (Fig. 6a). The northerly wind anomaly in the eastern flank of the anticyclonic circulation anomaly effectively decreases the prevailing southerly flows over the Great Plains along the western edge of the Bermuda High (Fig. 7). Climatologically, these prevailing southerlies bring moisture from the Gulf of Mexico to the Great Plains [*Arritt et al.*, 1997; *Helfand and Schubert*, 1995; *Higgins et al.*, 1997]. Thus, the anticyclonic circulation anomaly that develops in the simulation without spectral nudging results in a decreased moisture supply (Fig. 7) and therefore suppressed precipitation over the southern Great Plains. Meanwhile, the cyclonic circulation anomaly over the southeast US leads to excessive precipitation over the region (Fig. 2c). Spectral nudging successfully eliminates those spurious circulation anomalies (Fig. 6b), leading to a spatial distribution of precipitation (Fig. 5a) much closer to that observed (Fig. 2a).

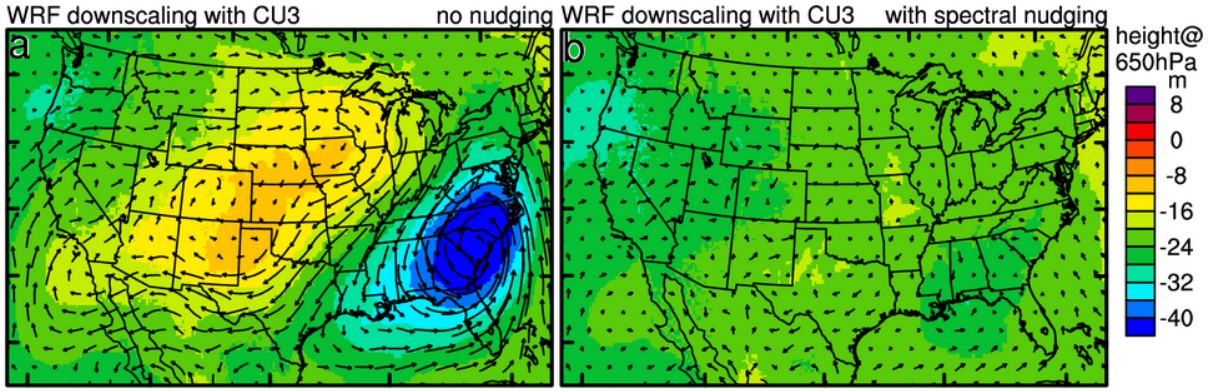

Fig. 6. Geopotential height difference during JJA 2005 between WRF downscaling and NCEP/DOE R2, (a) without and (b) with spectral nudge.

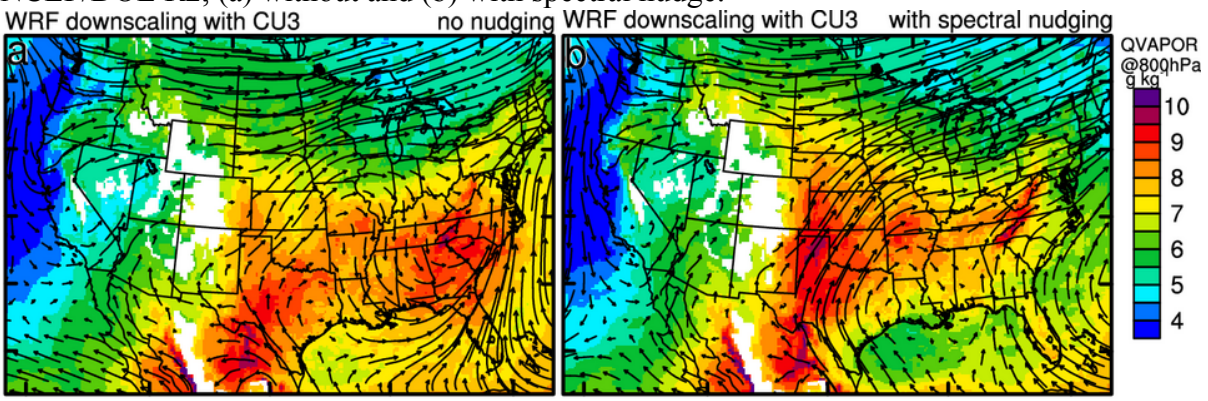

Fig. 7. Downscaled water vapor mixing ratio (QVAPOR) and wind fields at 800 hPa during JJA 2005 (a) without and (b) with spectral nudge.

Note that the downscaled WRF simulations have systematically lower geopotential heights than NCEP/DOE R2 fields by about 20 m across the whole domain (Fig. 6). This bias may be due to different vertical coordinate systems between WRF and NCEP/DOE R2. There are also some noisy differences of geopotential height between WRF and NCEP/DOE R2 along the boundary where mountains reside. Note that terrain heights used in WRF are interpolated by the WRF Preprocessing System (WPS), which differ from that of the modeling system used to produce the reanalysis data; such differences are more pronounced in mountainous regions [*Gochis et al.*, 2003].

6.2. Impact of different physics schemes

a) Impact on precipitation amount

With the large-scale circulations more accurately simulated by applying spectral nudging, the sensitivity of regional climate downscaling to different physics schemes can be examined in a more meaningful way. With spectral nudging always turned on, we run the JJA 2005 simulations with different physics parameterizations. To show only the most important similarities and differences, Fig. 5 highlights results from representative simulations for each parameterization category (e.g., PBL) or simulations with prominent differences from the base simulation. Different cumulus schemes are found to lead to more pronounced differences than other physics schemes tested in terms of precipitation amounts over the Great Plains. Previous studies [e.g., *Argueso et al.*, 2011; *Flaounas et al.*, 2011; *Jankov et al.*, 2005; *Lynn et al.*, 2009; *Sikder and Hossain*, 2016; *C X Zhang et al.*, 2011] at non-convection-permitting/resolving resolutions have also found stronger sensitivity of simulated cloud and precipitation to cumulus schemes than to other physics schemes such as the PBL, microphysics schemes. In particular, the BMJ (CU2), new SAS (CU14) and Tiedtke (CU6) schemes simulate substantially lower precipitation over the Great Plains than other cumulus schemes (Fig. 5), which is consistent with *F X Qiao and Liang* [2015]. It was speculated that cumulus schemes originally developed and often used in coarse-resolution GCMs (e.g., Tiedtke in the ECMWF global model, new SAS in the NCEP's Global Forecast System) are more likely to systematically underestimate the summer rainfall amount over the Great Plains [*F X Qiao and Liang*, 2015]. Recent modifications to the convective cloud-base mass flux, convective inhibition, and convective detrainment processes in the new SAS, some addressing scale dependency (scale awareness), were reported to lead to stronger precipitation and better-organized precipitation patterns, thus can potentially improve precipitation simulation [*Kwon and Hong*, 2017; *Lim et al.*, 2014].

The underestimated precipitation rate and widespread precipitation area produced by the BMJ scheme (Fig. 5b) agree with the well-known characteristic of the scheme. The BMJ scheme uses a profile-relaxation approach to adjust the simulated sounding toward a post-convective reference profile [*Betts*, 1986; *Betts and Miller*, 1986; *Janjic*, 1994]. BMJ was previously reported to often lead to a too dry conditions [*Gochis et al.*, 2002; *Jankov et al.*, 2005] and generate large areas of light rainfall while

severely underestimate summertime precipitation rates over US [*Gallus*, 1999] and Europe [*Pieri et al.*, 2015].

Multi-scale KF (CU11) leads to lower precipitation (3.6 mm day^{-1}, with NMB of -9.7%) over the Great Plains than the KF (CU1) scheme (4.14 mm day^{-1}, with NMB of 3.1%), which is consistent with the original design of the multi-scale KF scheme to reduce the excessive precipitation sometimes presented in weather forecasts with the KF scheme [*Zheng et al.*, 2016]. The KF scheme uses a mass flux approach to rearrange mass in an atmosphere column to remove at least 90% of the convective available potential energy (CAPE) [*Kain*, 2004]. Unlike the BMJ scheme that is primarily driven by the thermodynamics of the simulated sounding, thus is not directly impacted by vertical motion, the KF scheme is more influenced by surface convergence and the resulting vertical motion [*Gallus*, 1999]. Thus, KF can be more easily activated than the BMJ scheme and consequently leads to more precipitation than BMJ [*Gochis et al.*, 2002]. Also KF may produce unrealistically deep saturated layers in post-convective sounding, which can lead to post-convective stratiform precipitation and overprediction of total precipitation [*Pieri et al.*, 2015]. To mitigate the precipitation overprediction, *Zheng et al.* [2016] together with *Herwehe et al.* [2014] designed the multi-scale KF scheme by introducing a few changes to the KF scheme, including subgrid-scale cloud–radiation interactions, a dynamic adjustment time scale, impacts of cloud updraft mass fluxes on grid-scale vertical velocity, and scale-dependent lifting condensation level–based entrainment. These changes appear to reduce precipitation as shown in Figs. 5c and 5d.

Two variants of the Grell cumulus scheme (i.e., Grell-Freitas and Grell-3) are available in WRF, both of which are improved versions of a stochastic scheme originally implemented by *Grell and Devenyi* [2002]. The Grell-3 (CU5) scheme spreads subsidence on neighboring grid points while the Grell-Freitas (CU3) scheme is based on a scale-aware method recently introduced by *A. Arakawa et al.* [2011]. The Grell-Freitas (CU3) scheme leads to lower precipitation (3.7 mm day^{-1}, with NMB of -6.8%) over the Great Plains than the Grell-3 (CU5) scheme (4.1 mm day^{-1}, with NMB of 2.0%), which is different from the sensitivity over Brazil, where Grell-Freitas produced slightly (barely discernable) more precipitation than Grell-3 [*Grell and Freitas*, 2014]. The different sensitivity to Grell-Freitas and Grell-3 in different regions may be due to the different characteristics of precipitation. Note that the simulations are conducted at a 20-km horizontal grid spacing in this study. The benefit of the scale-aware Grell-Freitas scheme may be more appreciable when applied to gray-zone resolutions (defined as 1-10 km in *Kwon and Hong* [2017], 4-10km in *A. F. Prein et al.* [2015], 4-15km in *Y Gao et al.* [2017]) where the assumption of conventional cumulus schemes (that is, convective clouds cover only a small fraction of the model grid cell) starts to break down but moist convections are not completed resolved yet [*Fowler et al.*, 2016]. Note that the gray-zone here is framed from the perspective of cloud microphysics, which is different

from the gray-zone defined from the perspective of turbulence [*Bryan et al.*, 2003; *Shin and Hong*, 2015; *Wyngaard*, 2004; *Zhou et al.*, 2017].

Different PBL schemes simulate different PBL thermodynamic and kinematic properties, which can cause differences in precipitation. In this case, however, altering PBL schemes does not lead to significant change in the precipitation amount (Fig. 5a). The relationship between PBL properties and subsequent precipitation is complicated [*C Klein et al.*, 2015; *Trier et al.*, 2008], especially during the warm season in the Great Plains, where the precipitation may be influenced by mesoscale vertical circulation, eastward propagating convection, and large-scale moisture advection [*Dai et al.*, 1999; *Findell et al.*, 2011; *Liang et al.*, 2006; *Martynov et al.*, 2013; *F X Qiao and Liang*, 2015; *Schumacher et al.*, 2013]. In addition, some PBL schemes have different treatments for stable and unstable boundary layers [*Xiao-Ming Hu et al.*, 2010; *Hu et al.*, 2013] and thus have different performances for different time of day, which further complicates the identification of the effect of different PBL schemes on precipitation.

One key aspect of PBL schemes is their vertical mixing strength [*Xiao-Ming Hu et al.*, 2010] which can be dictated by a few important parameters in the schemes [*Hu et al.*, 2012; *P M Klein et al.*, 2016; *Nielsen-Gammon et al.*, 2010]. We chose to examine the sensitivity of a critical parameter in the YSU scheme that controls the daytime vertical mixing strength (p, an exponent affecting the magnitude and vertical distribution of eddy diffusivity within the PBL) identified by *X.-M. Hu et al.* [2010]. Results show that larger values of p lead to weaker vertical mixing and lower PBL heights, consistent with the formulation of eddy diffusivity [*Xiao-Ming Hu et al.*, 2010]. Consequently, lower PBL heights lead to more moisture near the surface and stronger CAPE in the afternoon. As a result, more precipitation is predicted in the afternoon, especially in the mountains and southeast U.S. (not shown). On the other hand, smaller values of p lead to higher PBL heights and consequently less precipitation. This sensitivity of simulated precipitation to different simulated PBL heights is consistent with the previous study of *Trier et al.* [2011].

Altering microphysics schemes does not change the precipitation amounts markedly, except that the Kessler scheme significantly under-predicts precipitation over most of the continent (Figure not shown) likely due to its complete ignorance of important ice microphysical processes.

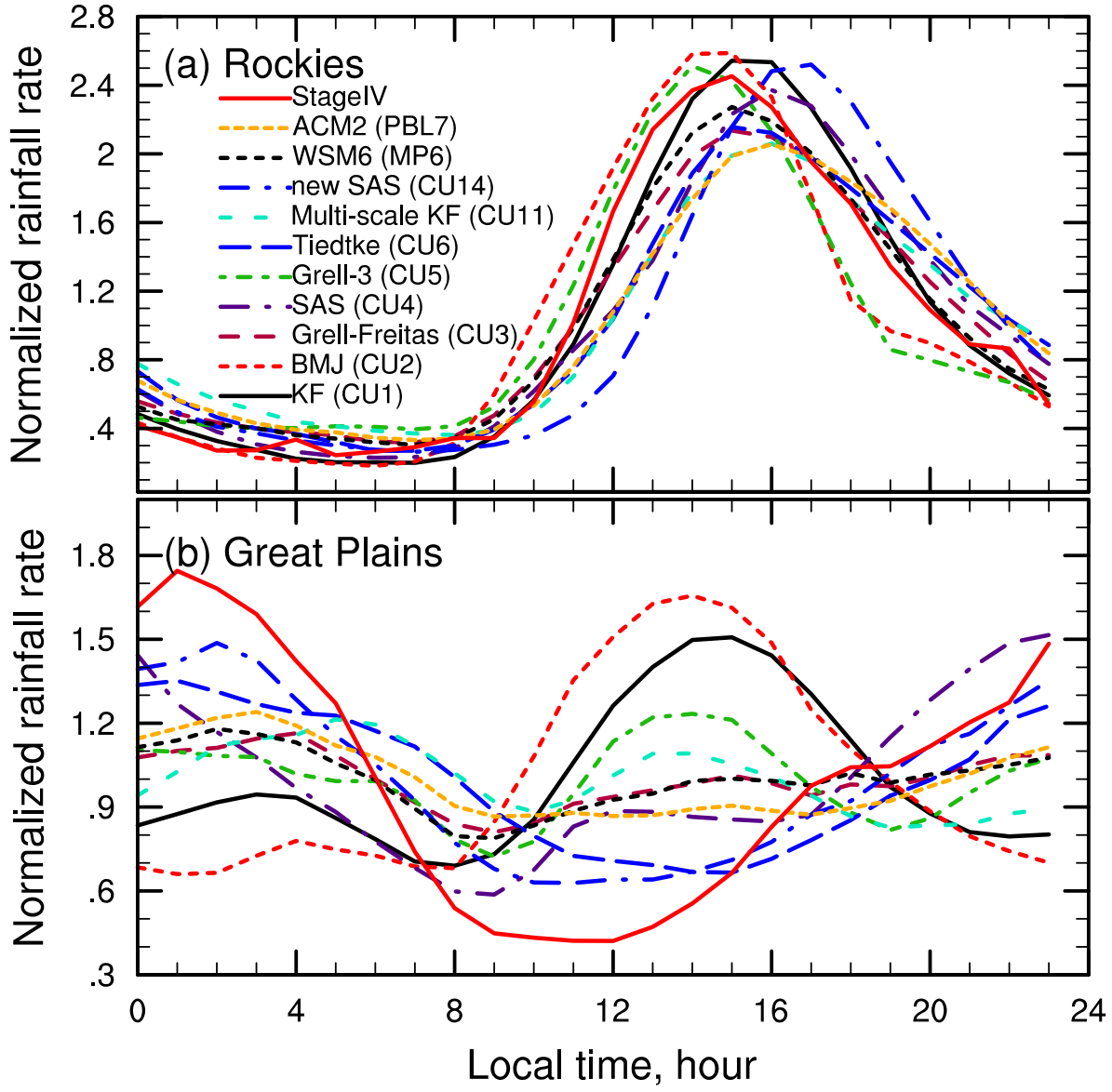

Fig. 8. Diurnal variation of normalized rainfall rate during JJA 2005 over the (a) Rockies and (b) Great plains. The hourly precipitation rate is normalized by the daily mean value, as in Liang et al. (2004b).

b) Impact on the diurnal variation of precipitation

Single-minded pursuit of the "best" performance in terms of total precipitation over the Great Plains may not be encouraged because some configurations may simulate the right amount of total precipitation but at wrong time. As seen in Fig. 1a, the precipitation across the Great Plains has unique diurnal and spatial variations, the precipitation peaks during nighttime and generally moves from west to east. Figure 8 shows the performance of 10 selected physics configurations in terms of the diurnal

variation of precipitation over the Rockies and Great Plains (the exact areas are marked using two boxes in Fig. 1a). Note that the hourly precipitation rate shown in Fig. 8 is normalized by the daily mean value, as in *Liang et al.* [2004]. Over the Rockies, all schemes predict peak precipitation in the afternoon, spanning from 1400-1700 local time, while the Stage IV product shows peak precipitation at 1500 local time (Fig. 8a). In contrast, the sensitivity of diurnal variation of precipitation to different parameterization schemes (particularly cumulus schemes) over the Great Plains is more pronounced (Fig. 8b). Altering PBL and microphysics schemes does not change diurnal variation of precipitation significantly, while cumulus parameterization strongly affects the diurnal variation of precipitation. The Stage IV data shows a prominent diurnal variation of precipitation over the Great Plains with daytime minimum and nighttime peak. The KF (CU1), BMJ (CU2), and Grell-3 (CU5) schemes erroneously place the peak precipitation over the Great Plains during the afternoon and miss the nighttime peak. The Grell-Freitas (CU3), new SAS (CU14), Multi-scale KF (CU11), and Tiedtke (CU6) capture the nighttime peak over the Great Plains. The behaviors of cumulus schemes are generally consistent with those seen in previous studies [*Leung and Gao*, 2016; *Liang et al.*, 2004; *Liang et al.*, 2006].

In summary, all the cumulus schemes perform relatively well over the Rockies and perform markedly differently over the Great Plains in terms of reproducing the diurnal variation of precipitation. These different performances are related to the characteristics of precipitation in different regions. Over the Rockies, the precipitation is dictated by (and peaks the same time as) boundary layer thermodynamic forcing such as surface fluxes and thermodynamic properties of the near-surface air, while the precipitation over the Great Plains is more governed by large-scale dynamic forcing such as free tropospheric advection/convergence [*M I Lee et al.*, 2007a; *G J Zhang*, 2003] and Low-Level Jets [*Harding et al.*, 2013]. It appears all the cumulus schemes perform fine over regions where precipitation is governed by boundary layer thermodynamic forcing, e.g., the Rockies (Fig. 8a) and the Southeast U.S. (figure not shown); while some cumulus schemes perform poorly over the Great Plains where peak precipitation is more in phase with large-scale forcing.

The closure assumption and trigger function adopted in cumulus schemes were reported to play a key role in dictating diurnal variation of precipitation [*Choi et al.*, 2015; *F X Qiao and Liang*, 2015; *Xie and Zhang*, 2000; *G J Zhang*, 2002; 2003]. Those closure assumptions and trigger functions that couple moist convection too strongly with boundary layer thermodynamic forcing and too weakly with large-scale forcing are likely to fail to accurately predict the observed nocturnal precipitation maxima over the Great Plains [*Liang et al.*, 2004; *F X Qiao and Liang*, 2015; *Xie and Zhang*, 2000]. For the two worst cumulus schemes in terms of simulated precipitation diurnal variation (i.e., KF and BMJ), a previous study [*F X Qiao and Liang*, 2015] has shown that the closure assumption of an instantaneous relaxation of thermodynamic profiles toward an quasi-equilibrium reference state, used in BMJ [*Baldwin et al.*, 2002; *Bukovsky et al.*, 2006; *Janjic*, 1994], and the assumption of CAPE being nearly completely removed by convection over a short time period (0.5-1 h), as in KF [*Kain*, 2004], are incapable of reproducing the correct timing of convection (i.e., the nighttime rainfall peak) in the Great Plains. Similar was also found by *Clark et al.* [2009] and *Leung and Gao* [2016] when comparing convection-allowing and convection-parameterized precipitation forecasts over the Great Plains.

For four other schemes that perform better in terms of diurnal variation of precipitation (i.e., Grell-Freitas (CU3), new SAS (CU14), Multi-scale KF (CU11), and Tiedtke (CU6)), the closure treatments are different. Grell-Freitas adopts a large-scale instability tendency closure, which is more sensitive to large-scale tropospheric forcing, in comparison to the KF scheme which is heavily influenced by the boundary layer forcing [*Liang et al.*, 2004]. Thus, the Grell-Fritsch scheme performs better over the Great Plains where the diurnal timing of convection is influenced by the large-scale vertical motion [*Dai et al.*, 1999]. For the new SAS scheme, a comprehensive convection trigger function is used, which evaluates two conditions for convection initiation: (1) the cloud base (defined as the level of free convection) must be within 150 hPa depth from the convection starting level (defined as the level of maximum moist static energy); and (2) the cloud work function (CWF) exceeds a critical CWF calculated as a function of the large-scale vertical velocity at the cloud base. This comprehensive trigger function was found to play a key role in reproducing the diurnal variation of precipitation over the Great Plains [*M*

I Lee et al., 2008; *Y C Wang et al.*, 2015]. The recent addition of the capability of scale-awareness to the KF scheme [*Alapaty et al.*, 2012; *Bullock et al.*, 2015; *Zheng et al.*, 2016], resulting in the multi-scale KF scheme, appears to enhance its performance in terms of reproducing the diurnal variation of precipitation over the Great Plains. The Tiedtke (CU6) scheme uses a trigger function based on the buoyancy of a undiluted parcel rising from near the surface and a CAPE removal closure based on large-scale convergence [*Nordeng*, 1995; *C X Zhang et al.*, 2011]; it nicely reproduces the diurnal variation of precipitation (Fig. 8), but significantly underestimates total amount of precipitation over the Great Plains (Fig. 5g), similar to previously reported [*F X Qiao and Liang*, 2015].

Precipitation from the Rockies to the Great Plains shows an eastward propagation (Fig. 1a, Fig. 9a). The KF (CU1) and BMJ (CU2) schemes that predict afternoon precipitation peaks over both the Rockies and Great Plains, barely reproduce any eastward propagation of precipitation in the region (Fig. 9b, c). On the other hand, the schemes that better reproduce the diurnal variation of precipitation across the Rockies and Great Plains (e.g., Grell-Freitas (CU3), Tiedtke (CU6), Multi-scale KF (CU11), new SAS (CU14)) also better capture the eastward propagation of precipitation (Fig. 9d, e, g, h). Particularly the scale-aware multi-scale KF scheme shows pronounced improvement over its non-scale-aware counterpart (i.e., KF).

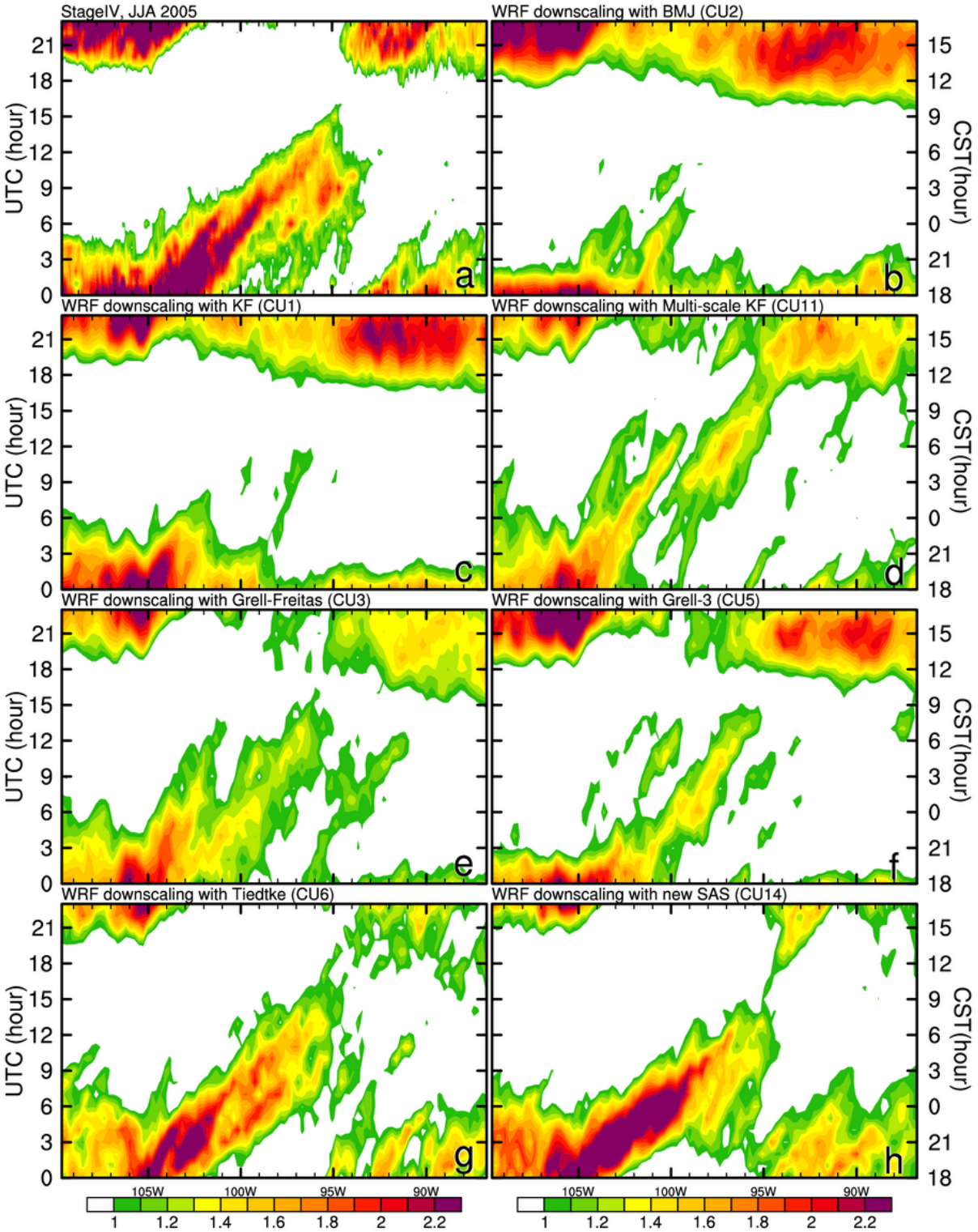

Fig. 9. Diurnally average Hovmoller diagrams of normalized hourly precipitation during JJA 2005 from (a) StageIV observed precipitation and WRF downscaling with different cumulus schemes, i.e., (b) BMJ (CU2), (c) KF (CU1), (d) Multi-scale KF (CU11), (e) Grell-Freitas (CU3), (f) Grell-3 (CU5), (g) Tiedtke (CU6), (h) new SAS (CU14).

6.3. 36-year (1980-2015) precipitation downscaling and comparison with the NARCCAP WRFG downscaling

Using what we learned from the prior numerical experiments for summer 2005, we use the control configuration of WRF model but with the inclusion of spectral nudging (hereafter refer to as nudging_WRF) to downscale precipitation from NCEP/DOE R2 reanalysis for a 36-year period (1980-2015). Figures 10 and 11 compare the downscaled monthly climatological precipitation from January-June and July-December, respectively, during the 36-year period with the PRISM precipitation data. The downscaled results capture the spatial distribution of climatological precipitation amount for each month as well as the monthly variation. Figure 12 shows the annual variation of precipitation amount over the Great Plains. Overall, the WRF downscaling captures the yearly variation of precipitation amount over the Great Plains with a correlation of 0.743 with the PRISM dataset, and it over-predicts the precipitation amount with a mean bias (MB) of 0.055 mm day^{-1} and a normalized mean bias (NMB) of 2.4%.

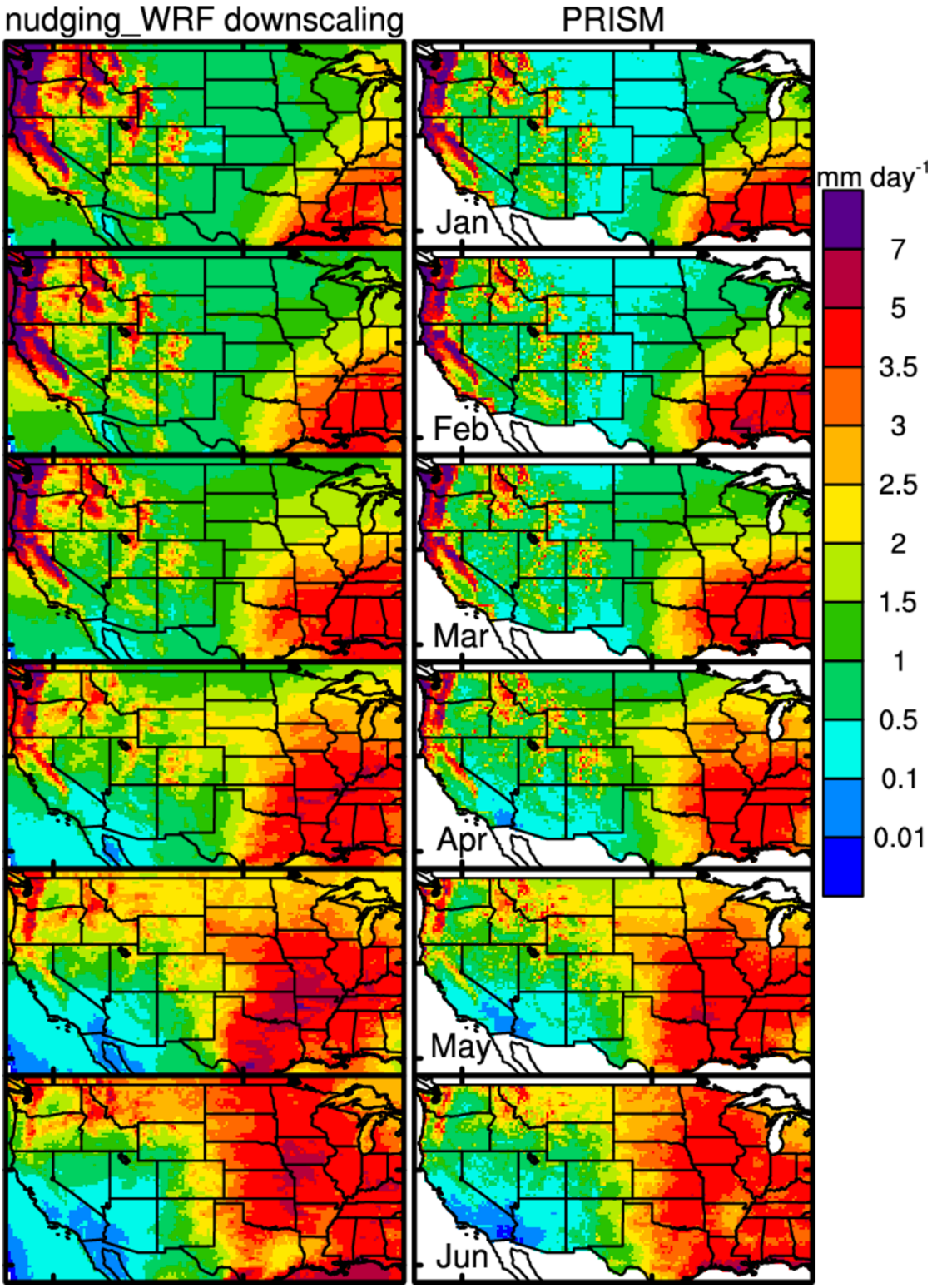

Fig. 10. 36-year (1980-2015) monthly climatological precipitation (left) dynamically downscaled with nudging_WRF and (right) retrieved from the PRISM data for the month (top to bottom) January through June.

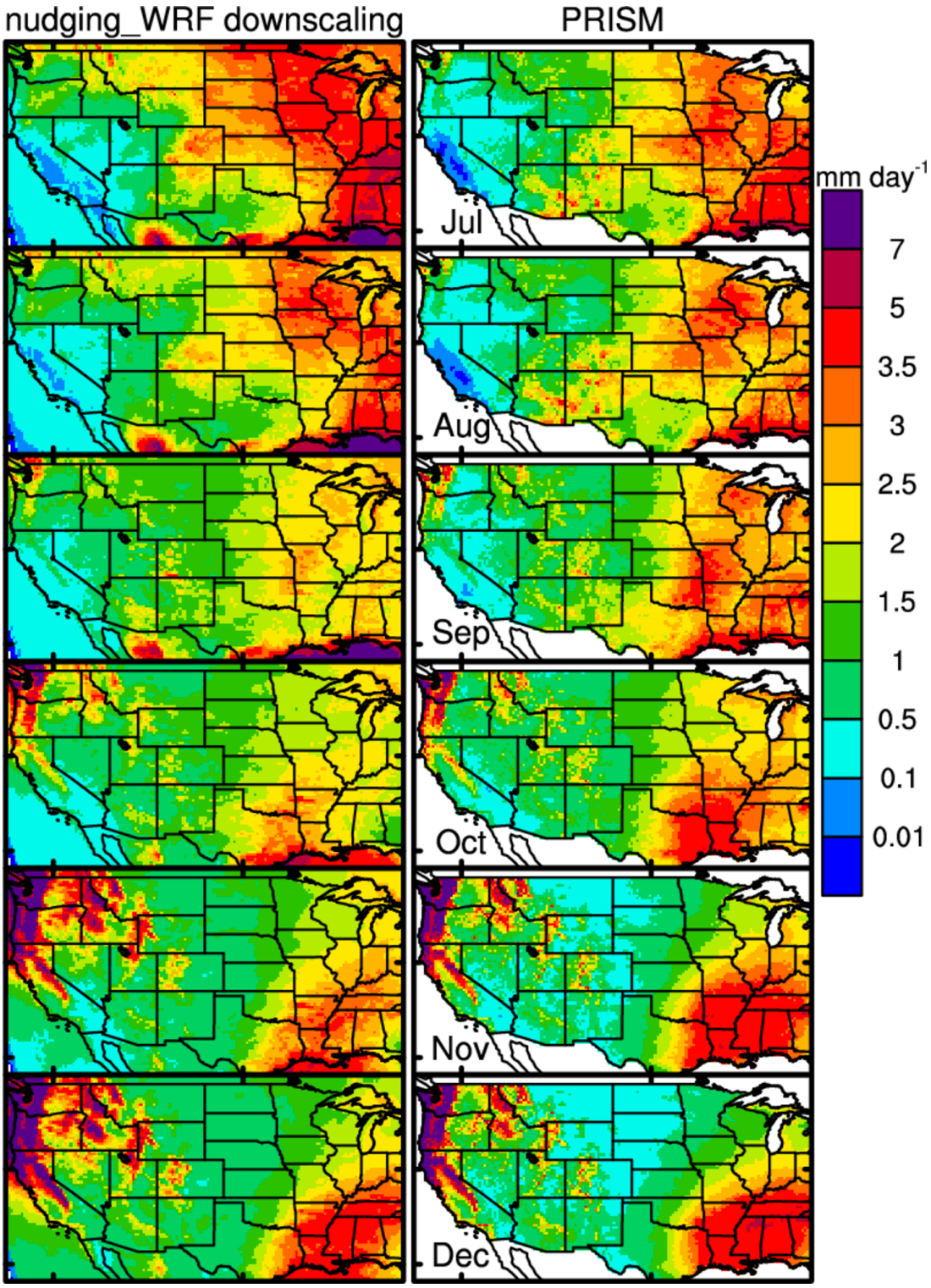

Fig. 11. Same as Fig. 10, but for the month (top to bottom) July through December.

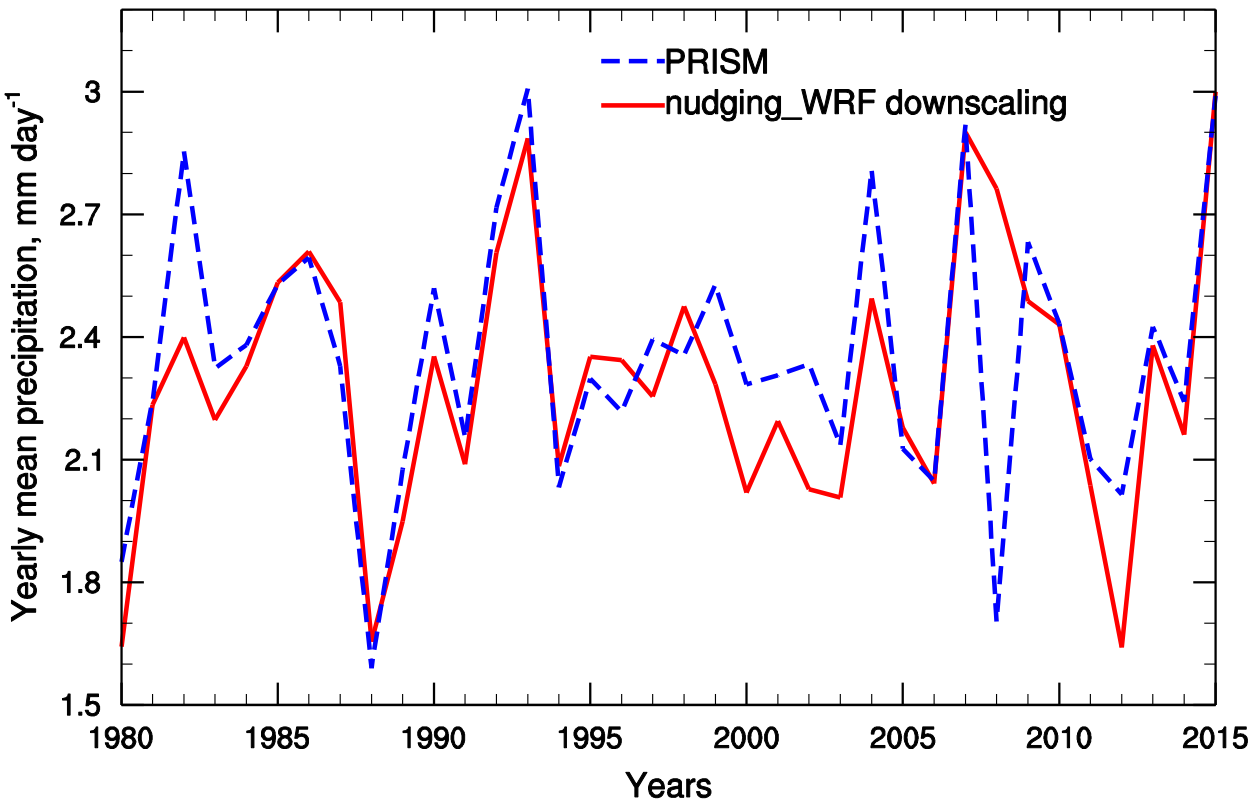

Fig. 12. Time series of observed and downscaled yearly mean precipitation rate for the 36-year period (1980-2015) over the Great Plains region, which is marked in the black box in Fig. 1.

We also compare the nudging_WRF downscaling results with those of the 25-year (1980-2004) NARCCAP WRFG to gauge the quality of downscaled precipitation. Note that spectral nudging is not applied in NARCCAP WRFG [*Mearns et al.*, 2012], and detailed configuration of WRFG can be found at http://www.narccap.ucar.edu/data/rcm-characteristics.html. The first 25-year subset of nudging_WRF downscaling is compared with the PRISM dataset and NARCCAP WRFG downscaling in Figs. 13, and 14. NARCCAP WRFG significantly under-predicts the monthly climatological precipitation over the Great Plains, especially for May through October (Fig. 15). In addition, in the months of July and August, NARCCAP WRFG simulates a spatial distribution of precipitation from the Rockies to Great Plains that is not correct (Fig. 14). The PRISM data show more precipitation over the Great Plains than over the Rockies while NARCCAP WRFG barely simulates any precipitation over the Great Plains and precipitation that is too high over the Rockies. The warm season dry biases of NARCCAP WRFG over the Great Plains may be related to the underestimated frequency of nocturnal southerly low-level jets [*Tang et al.*, 2016]. As noted earlier, we saw similar poor performance in our previous downscaling experiments without spectral nudging [*X Sun et al.*, 2016]. With a carefully designed configuration in this current study, however, nudging_WRF provides a better precipitation downscaling over CONUS in nearly every month (Figs. 13, 14), even though it moderately over-produces precipitation over the Great

Plains for certain months (particularly May and June, Fig. 15). We are also able to substantially alleviate the bias in precipitation locations in warm months (particularly July and August), as compared with those in NARCCAP WRFG and Sun et al. (2016). For example, the mean bias of precipitation of NARCCAP WRFG over the Great Plains (-0.723 mm day^{-1}, -32.1%) is reduced to 0.092 mm day^{-1} (4.1%) in this study.

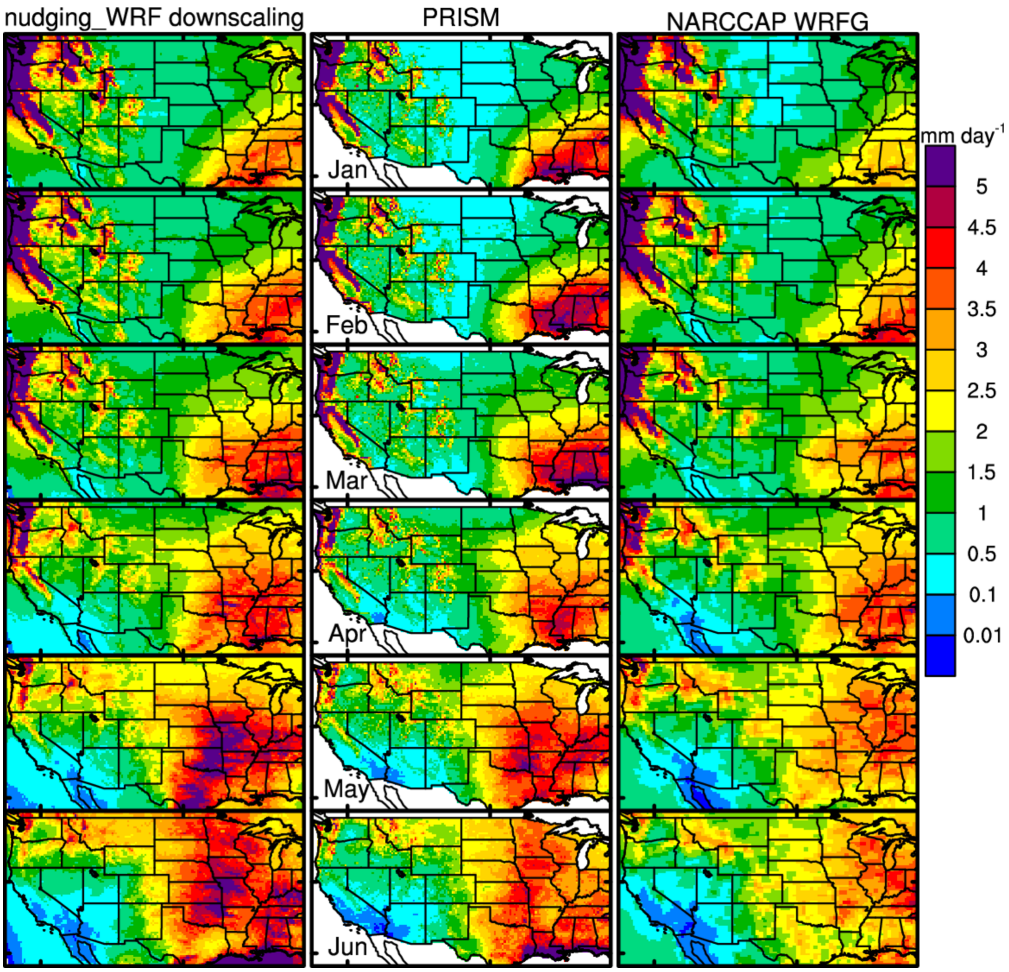

Fig. 13. 25-year (1980-2004) monthly climatological precipitation dynamically downscaled (left) with nudging_WRF in this work and (right) with NARCCAP WRFG, and (middle) retrieved from the PRISM data for the month (top to bottom) January through June.

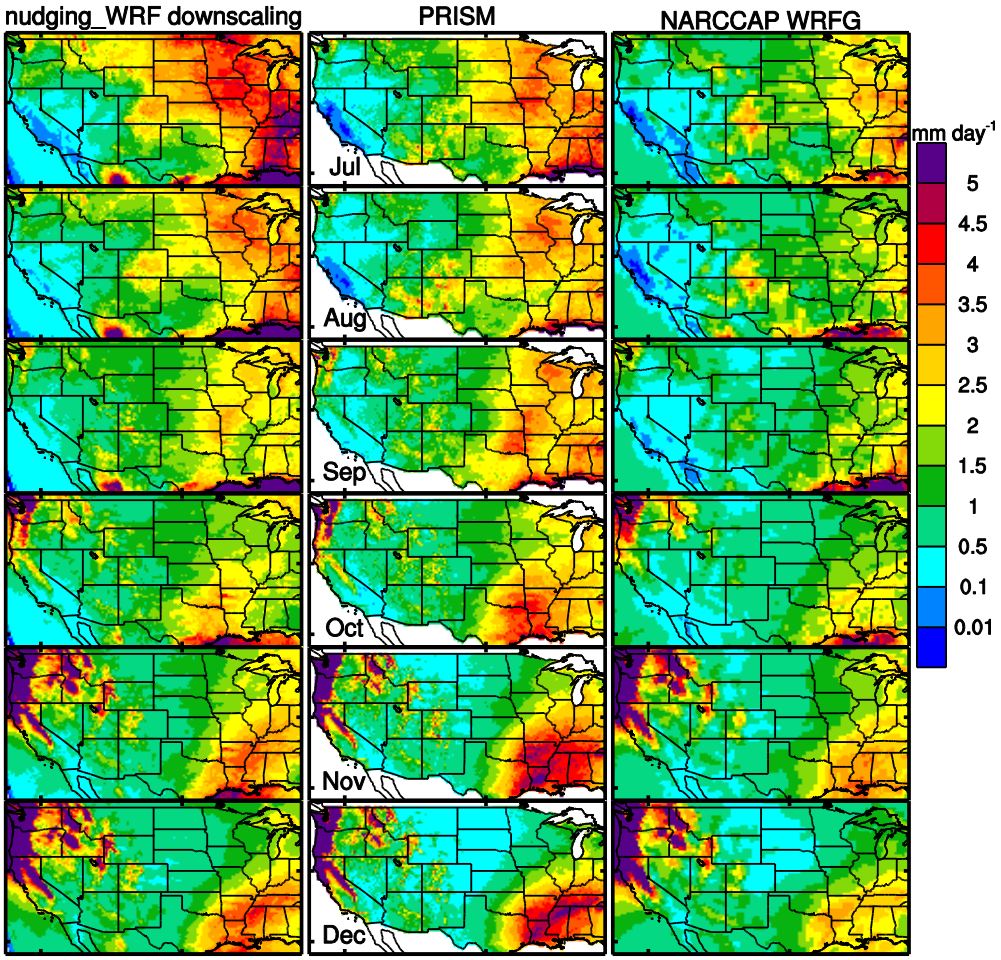

Fig. 14. Same as Fig. 13, but for the month (top to bottom) July through December.

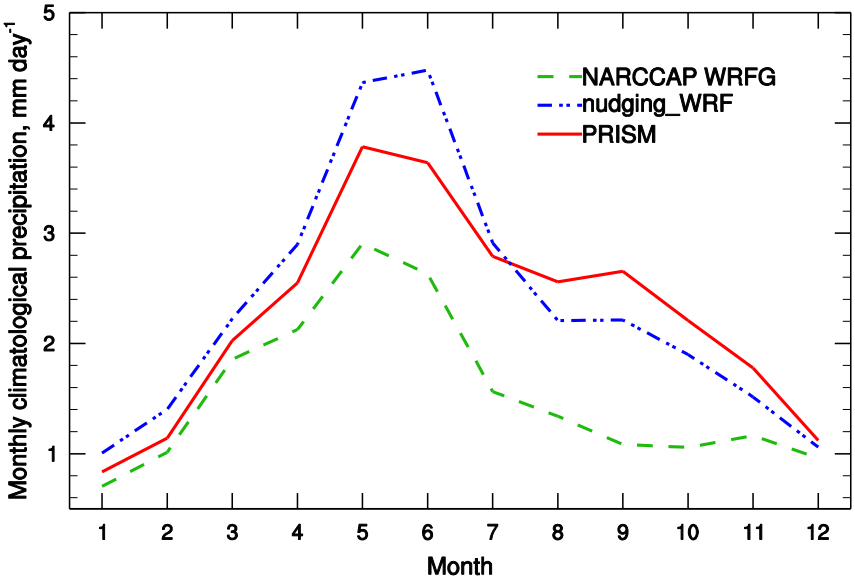

Fig. 15. Time series of monthly climatological precipitation rate during the 25-year period (1980-2004) over the Great Plains observed in the PRISM data and downscaled with nudging_WRF in this study and NARCCAP WRFG.

6.4 *Impact of the improved downscaling on hydrological assessment*

L Qiao et al. [2014b] demonstrated large uncertainties in the hydrological response of the trans-state Oologah Lake watershed in the Great Plains to the NARCCAP-downscaled output. Here we examine the impact of our improved precipitation downscaling on the hydrological response in this watershed.

We calculated monthly streamflow at the outlet of the Oologah Lake watershed for 1990-1999 using the VIC model driven by either our improved precipitation downscaling or that of NARCCAP WRFG. Due to the significant underestimation of precipitation over the Great Plains (Fig. 15), the NARCCAP WRFG-driven VIC simulation shows a significant underestimation of the streamflow at the watershed outlet (that is the Verdigris River near Lenapah, Oklahoma) over most of the time period. Most significant underestimation occurs in years 1994, 1995, 1998, 1999, and 1992-1993. With the improved downscaled precipitation from this study, the simulated monthly streamflow rates have a much better agreement with observations. The correlation between observed and simulated streamflow rates is improved from about 0.4 to 0.6 and the normalized mean bias is improved from -75% to 28%.

6.5 *using downscaling results and precipitation data to investigate impact of Edwards Plateau on precipitation in Texas*

Using the above validated configuration, WRF downscaling simulations with a 4km resolution for August of 2002-2015 were conducted to investigate impact of Edwards Plateau on precipitation in Texas, together with the Stage IV precipitation data

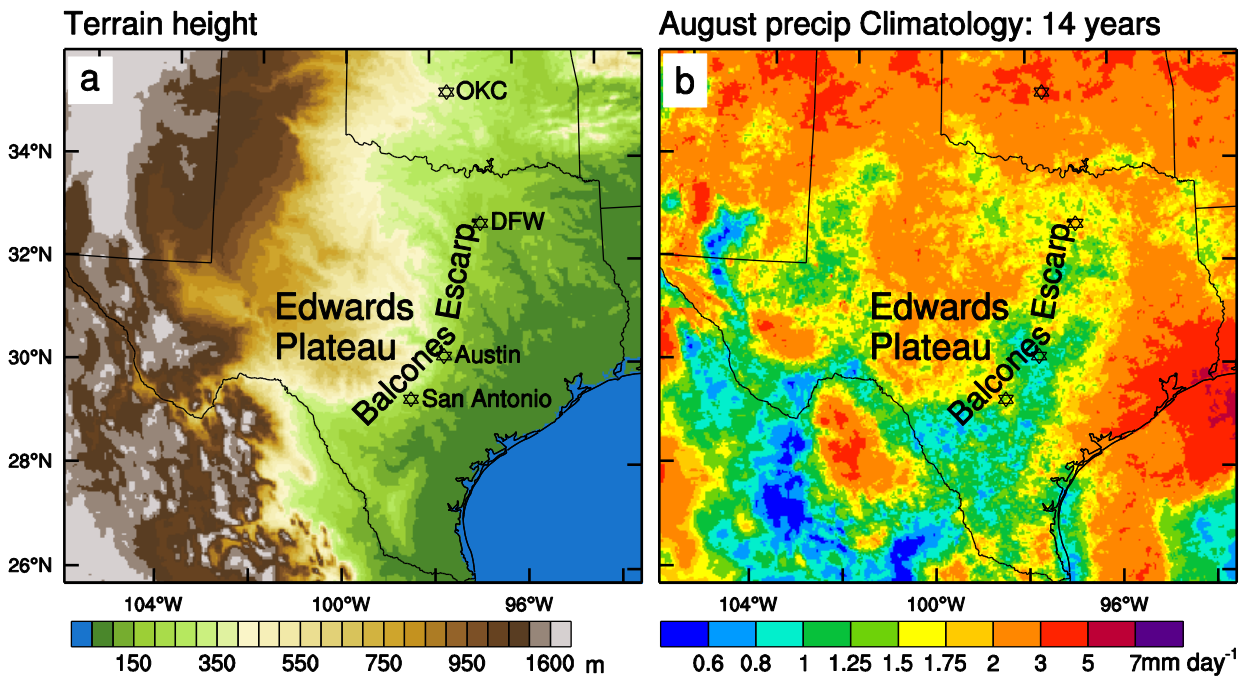

Fig. 16. (a) Terrain height in Texas and (b) climatological precipitation in August during 2002-2015 retrieved from the Stage IV data. The three main metropolitan areas located along the Balcones Escarpment, i.e., San Antonio, Austin, and Dallas-Fort Worth (DFW), are marked.

Based on our analysis of 14-year (i.e., 2002-2015) Stage IV precipitation data, the impact of the Edwards Plateau on the spatial distribution of precipitation is most prominent in August (Fig. 16b), probably due to strong radiative heating and fewer disturbances by strong synoptic scale transient processes (e.g., synoptic cold fronts). In this month, the total precipitation east of the Balcones Escarpment is suppressed as compared to that across the Edwards Plateau. Particularly at 1500 Central Standard Time (CST) (2100 UTC), the precipitation maximum over the Edwards Plateau appears distinct from the elongated precipitation minimum east of the escarpment (Figure not shown). The precipitation gradient corresponds to the terrain of the Edwards Plateau (more precisely, the position of the Balcones Escarpment), suggesting that the Edwards Plateau and Balcones Escarpment play some roles in modifying the spatial distribution of precipitation in the region.

Mountains have been reported to affect precipitation in many places around the world through the mountains' thermal effect or orographic forcing effect [e.g., *Bao and Zhang*, 2013; *Carbone and Tuttle*, 2008; *Y X Gao et al.*, 1981; *He and Zhang*, 2010; *X D Liu et al.*, 2009; *J H Sun and Zhang*, 2012; *Tripoli and Cotton*, 1989b; *Q W Wang et al.*, 2016; *Wolyn and Mckee*, 1994; *Y C Zhang et al.*, 2014]. On a clear summer afternoon, because of absorption of strong

shortwave radiation, elevated terrain acts as a heat source, warming the near-surface air over the higher terrain as compared to adjacent, low-lying areas and producing a baroclinicity. As a result, a shallow (~4 km AGL) solenoid develops, comprised of an upslope wind along the sloping terrain and a downward return flow over the adjacent, lower elevations. This thermally driven, local to regional scale circulation is commonly known as the Mountain-Plains Solenoid (MPS) circulation [*Hu and Xue*, 2016; *Hu et al.*, 2014; *Tripoli and Cotton*, 1989a; *Wolyn and Mckee*, 1994]. During the night, due to radiative cooling, the thermal gradient between mountains and the adjacent low-laying ground is reversed, as is the MPS circulation. The upward branch of the MPS circulation (over the mountains during the day and over the adjacent low-lying ground during the night) normally enhances precipitation [*He and Zhang*, 2010]. In most of the documented cases of precipitation modulation by the MPS circulation, the elevation difference (e.g., the Rockies, Tibetan Plateau, Loess Plateau) is greater than that between the Edwards Plateau and coastal plains. For the latter, the elevation difference is only 500-700 m (Fig. 16a). Thus, we need to carefully examine the possible causes of the precipitation maximum over the plateau.

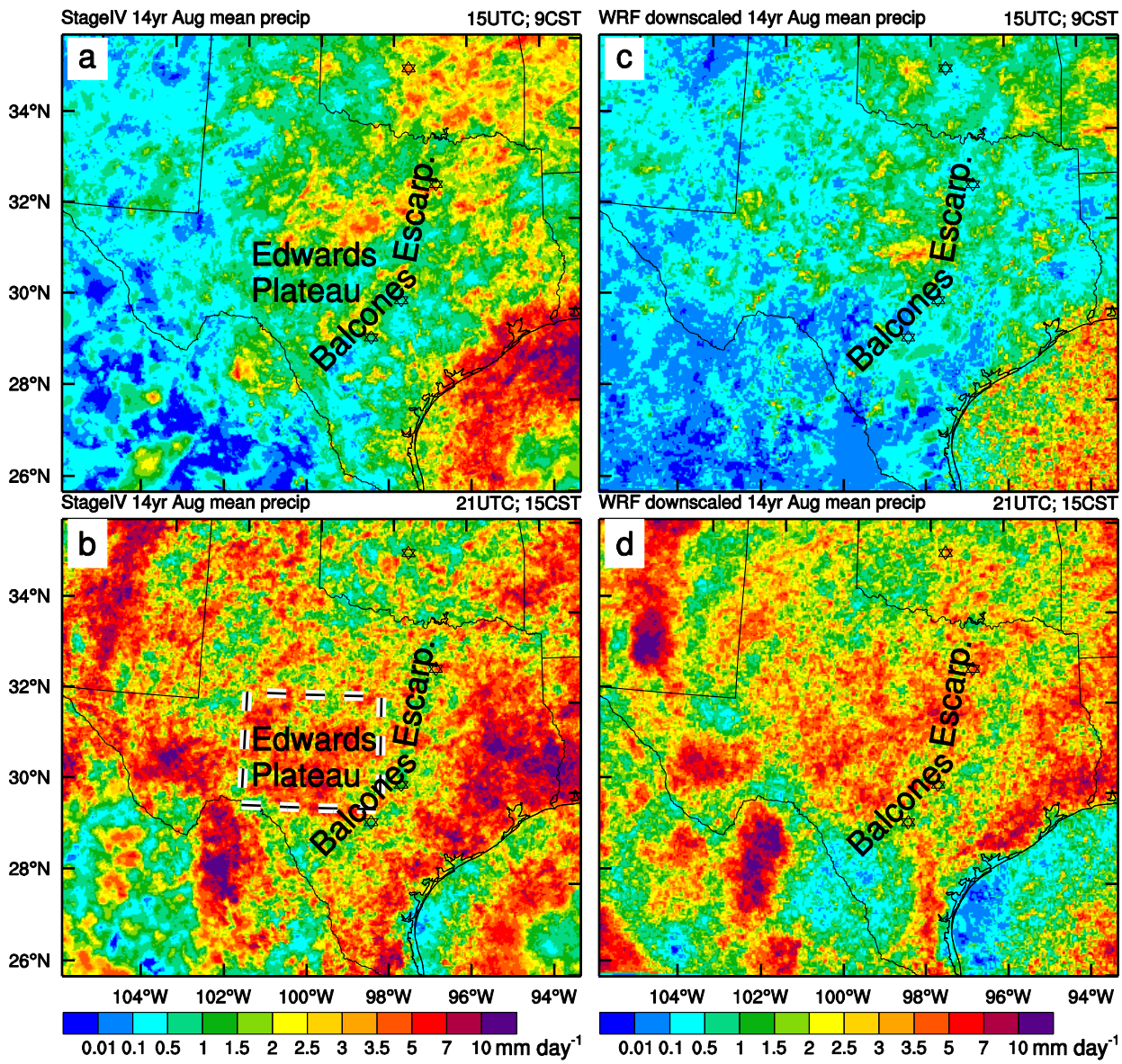

Fig. 17. Mean hourly precipitation rate (in mm day^{-1}) for August 2002-2015 (left) retrieved from the Stage IV data and (right) downscaled by WRF at (top) 0900 and (bottom) 1500 CST.

Since the thermal effect of any mountains has distinct diurnal variation [*He and Zhang*, 2010], simply focusing on the daily mean precipitation may obscure the different effects at different time of the day. Thus, we examined the frequency and rate (Fig. 17) of the hourly precipitation. Although the hourly precipitation rate is underestimated in the model simulations (as compared to the Stage IV data) at 0900 CST, the values and spatial patterns are realistic by 1500 CST (Fig. 17). Precipitation over the Edwards Plateau showed a prominent diurnal variation, with a dominant peak in the afternoon (1500-1800 CST) and a secondary peak in the early morning, 0700-0900 CST (Fig. 18).

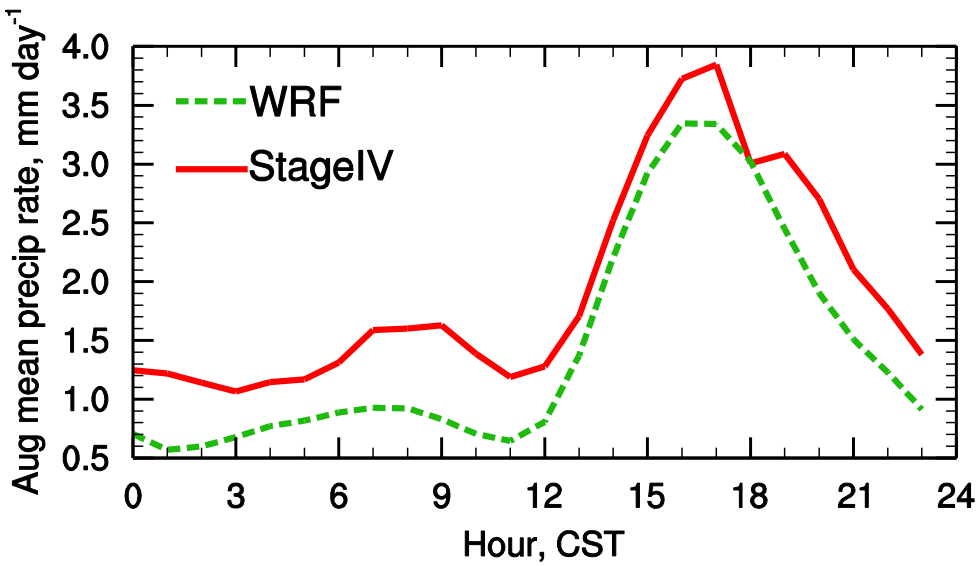

Fig. 18. Time series of hourly precipitation rate (in mm day^{-1}) averaged over the Edwards Plateau domain marked by dashed lines in Fig. 17b.

The smaller, early morning peak in precipitation results from the eastward propagation of mesoscale convective systems (MCSs) initiated in the Rockies on the previous afternoon. The eastward propagation of MCSs provides the dominant nighttime precipitation in the central United States [*Dai et al.*, 1999; *S A Klein et al.*, 2006; *F X Qiao and Liang*, 2015]. Because the Edwards Plateau is near the southern and eastern extent of the nighttime propagation of these mesoscale features off of the Rockies, it receives the associated precipitation during the early morning. The model successfully captures the timing of the eastward propagation of precipitation systems, but underestimates the precipitation intensity (Figs. 17c). It appears that the simulated precipitation maximum becomes weaker than observed during the eastward propagation process (Fig. 17a vs. 17c), leading to an early morning dry bias over Texas (Fig. 18), which is consistent with previously dynamic downscaling studies [*Berg et al.*, 2013; *Harris and Lin*, 2014; *S A Klein et al.*, 2006; *M I Lee et al.*, 2007b; *Ma et al.*, 2014; *Tripathi and Dominguez*, 2013].

The dominant afternoon peak is presumably due to the locally initiated moist convection [*Liang et al.*, 2004]. Both the hourly frequency (Figure not shown) and amount (Fig. 17b) of afternoon precipitation shows a coherent spatial pattern, with most precipitation events occurring in the eastern half of the Edwards Plateau and the precipitation east of the Balcones Escarpment suppressed, consistent with the spatial distribution of daily mean precipitation shown in Fig. 16b. The consistency between the daily mean precipitation and afternoon hourly precipitation

indicates that the afternoon moist convection plays a dominant role in determining the spatial distribution of precipitation over this region of Texas in August. The dynamic downscaling results capture the spatial pattern of both afternoon precipitation frequency and amount. Although the simulations significantly overestimate precipitation frequency, the model accounts for all non-zero precipitation while very light precipitation may not be recorded in the Stage IV data; this may partially explain the overestimation of frequency of afternoon precipitation in the model.

By examining the resemblance between hourly precipitation patterns and topography, the Edwards Plateau and Balcones Escarpment appear to play a great role in modulating afternoon precipitation, i.e., in enhancing the afternoon precipitation over the eastern Edwards Plateau and suppressing the afternoon precipitation east of the Balcones Escarpment. Since the WRF model successfully captures the general characteristics of the precipitation over Texas, confidence is gained for us to investigate the specific factors that modulate the precipitation patterns based on the modeling results. The afternoon precipitation gradient across the plateau, escarpment, and plains corresponds well with the simulated upward motions. We first hypothesize that the upward branches of the MPS circulation enhances the afternoon precipitation, as reported in many previous studies [e.g., *He and Zhang*, 2010]. However, the spatial distribution of vertical velocity contradicts such a hypothesis: the upward motion does not occur in the region with the largest slope (i.e., western side of the Edwards Plateau) as the MPS circulation would. Instead, upward motion occurs in some regions with a gentle slope, e.g., east of Dallas-Ft. Worth (DFW). Therefore, the MPS circulation associated with the sloping terrain does not provide a good explanation on the main upward motion found in the model.

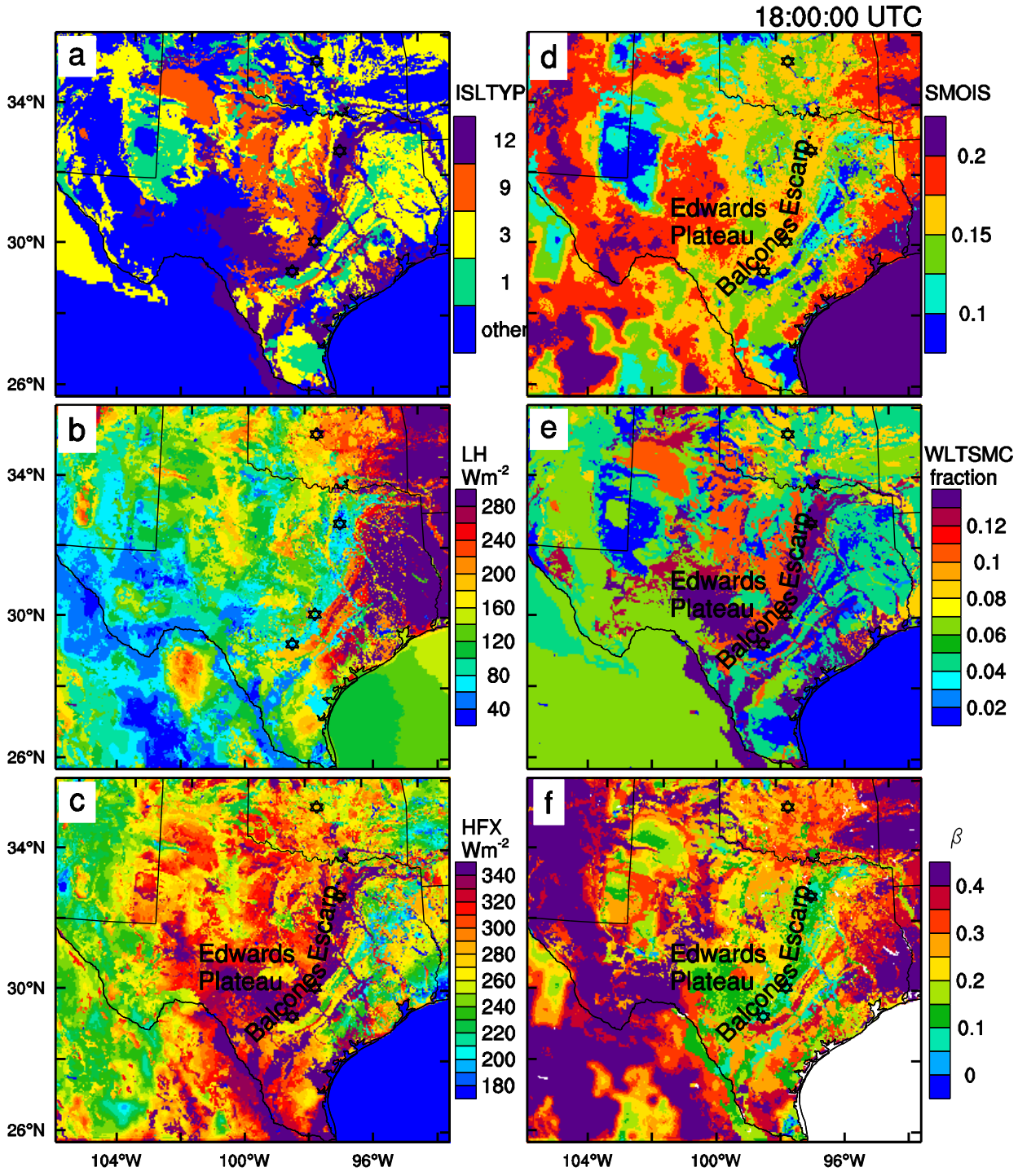

Fig. 19. Spatial distribution of (a) soil types, (b) latent heat flux (LH, in W m^{-2}), (c) sensible heat flux (HFX, in W m^{-2}), (d) soil moisture (SMOIS, in fraction) (e) wilting soil moisture content (WLTSMC, in fraction), and (f) moisture availability parameter (β) at 1200 CST.

Land surface processes are examined to search for the possible reasons for the specific pattern of the upward motions over the Edwards Plateau. It turns out that the spatial pattern of vertical velocity matches that of sensible heat flux over the Edwards Plateau (Fig. 19c), which is further tied to the soil type (Fig. 19a). Dominant soil types 9 (clay loam) and 12 (clay), found underneath the upward motion over the Edwards Plateau, lead to relatively low latent heat fluxes and relatively high sensible heat fluxes while the dominant soil types 1 (sand) and 3 (sandy loam), found underneath the downward motion east of the Balcones Escarpment, lead to relatively high latent heat fluxes and relatively low sensible heat fluxes. Soil moisture alone cannot explain the spatial distribution of latent and sensible heat fluxes. Soil moisture over soil types 9 (clay loam) and 12 (clay) is actually higher than soil types 1 (sand) and 3 (sandy loam) east of the Balcones Escarpment (Fig. 19d); however, the latent heat fluxes over clay-based soil types (9 and 12) are lower and sensible heat fluxes are higher.

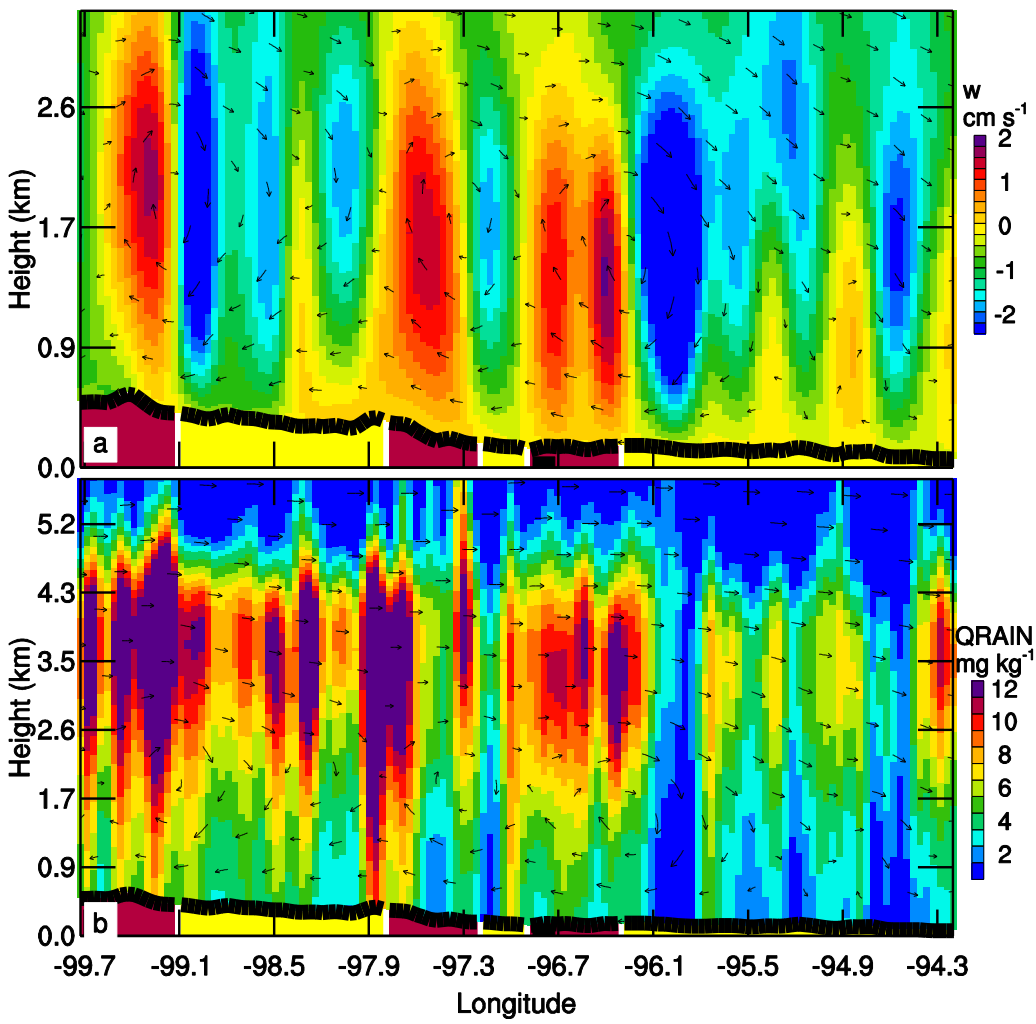

Fig. 20. West-to-east cross sections of (a) vertical velocity (w, in cm s^{-1}) and (b) rain water mixing ratio (QRAIN, in mg kg^{-1}) through Dallas, Texas at 2100 UTC (1500 CST). The dominant soil types are shaded under the thick black line, which indicated the terrain surface. The clay-based soil types 9 and 12 are shaded in dark red-brown; sand-based types 1 and 3 are shaded in yellow. Wind vectors are overlaid on each plot. Note that vertical velocity is multiplied by 100 when plotting wind vectors. The longitudinal position of Dallas (–96.8˚) is marked by a black rectangle on the x-axis.

To examine these relationships in more detail, we reviewed the hydraulic properties of different soil types used by the WRF model. The marked differences between clay-based soil types 9 and 12 and sand-based soil types 1 and 3 are with the dry-soil moisture threshold (DRYSMC) and wilting-point soil moisture (WLTSMC) of the soil. For any given soil type, the Noah land-surface model uses the same value for these two parameters. These parameters play an important role in dictating evapotranspiration by scaling potential evapotranspiration through a moisture availability parameter β [*Betts et al.*, 1997; *Chen and Dudhia*, 2001]:

$$\beta = \frac{\Theta - \Theta_w}{\Theta_{ref} - \Theta_w} \qquad (1)$$

where Θ is volumetric soil moisture content, Θ_{ref} is the field capacity, and Θ_w is either the soil moisture at the wilting point (WLTSMC) for vegetation canopy evapotranspiration or the dry-soil moisture threshold (DRYSMC) for ground surface direct evaporation. When the soil moisture becomes lower than DRYSMC or WLTSMC, β is set as zero and surface evapotranspiration is shut off. The clay-based soil types have higher values of DRYSMC and WLTSMC than sand-based types (Fig. 19e), by a factor of as high as 14. Because DRYSMC and WLTSMC values can be high (as high as 0.138 m^3 m^{-3}) for clay-based soil types (which dominate over the eastern Edwards Plateau), the actual soil moisture values are more likely to decrease below the DRYSMC and WLTSMC of clay-based as opposed to sand-based soils, leading to nearly zero β (Fig. 19f) for the former soil types. Thus, one would expect lower latent heat fluxes (Fig. 19b) and consequently high sensible heat fluxes in regions with clay soils (Fig. 19c).

The simulated different behavior of surface fluxes over clay and sand is consistent with soil granulometry. Sand is composed of relatively coarse particles with diameter between 2 mm and 50 μm while clay is composed of fine particles with diameter less than 2 μm [*S Liu et al.*, 2013]. Sandy soil is coarse textured, allowing water to easily circulate via capillary motion to reach the surface or plant roots where it can be evaporated or absorbed (and eventually released

from leaves) [*Fast and Mccorcle*, 1990; *Mahfouf et al.*, 1987]. In contrast, in fine textured clay soil, the capillary motion is quite slow and it is hard for water to circulate and participate in evapotranspiration, thus leading to suppressed latent fluxes (consequently enhanced sensible heat fluxes) during the day [*Fast and Mccorcle*, 1991; *Mahfouf et al.*, 1987]. The high sensible heat fluxes over clay-based soils (Fig. 19c) will induce upward motion that helps to trigger the afternoon moist convection under favorable conditions.

The west-to-east vertical cross-sections of vertical velocity and rain water through DFW further corroborate the above analysis (Fig. 20). Upward motion occurs almost exactly over the clay-based soil types (shaded in dark red-brown) while downward motion occurs over the sand-based soil types (shaded in bright yellow), with a solenoidal circulation being the strongest along the clay-sand boundaries (Fig. 20a). Latent heat flux is more (less) likely to shut down over the clay- (sand-) based soil due to its high (low) values of DRYSMC and WLTSMC, consequently leading to high (low) sensible heat flux and upward (downward) motion. The resulting downward motion over the sandy soils suppresses the precipitation east of DFW while the upward motion over the clay soils triggers more precipitation west of the Balcones Escarpment (Fig. 20b). The impact of different surface energy balance (or partition between sensible and latent heat fluxes) on precipitation shown in this study is also corroborated by large eddy simulations conducted by *Kang* [2016], in which a higher Bowen ratio (i.e., more sensible heat flux relative to latent flux) is shown to more likely trigger afternoon moist convection. This study is also consistent with previous observational studies [e.g., *Taylor et al.*, 2012] that show more afternoon rainfall over areas with enhanced sensible heat flux.

Due to the companion presence of upward and downward motions, local circulations (named as soil-type circulation) are developed over some regions, e.g., east of DFW. A similar local circulation due to a comparable spatial pattern of vertical velocities along the Balcones Escarpment was previously reported in a case study on 7 August 2011 where the local circulations were, however, attributed to the MPS circulation as a result of the terrain height difference [*Hu and Xue*, 2016]. Yet, the gentle terrain slope east of DFW (Fig. 20) disproves the MPS circulation hypothesis but corroborates the soil-type circulation idea.

7. analysis and findings

- With the optimized configuration, WRF model downscaling is carried out from NCEP/DOE R2 forcing for a 36-year period (1980-2015) over the CONUS domain.
- The downscaling obtained from this study captures well the spatial/temporal variation of monthly climatology precipitation
- Different cumulus schemes lead to more pronounced difference in simulated precipitation than other tested physics schemes at a 20 km grid spacing
- Spectral nudging is important for correctly downscaling precipitation over the Great Plains.
- High dry-soil moisture threshold and wilting-point soil moisture trigger more afternoon moist convection over the Edwards Plateau in August
- We obtained a better understanding of the band of afternoon, near-surface wind maxima along the Balcones Escarpment
- The soil-type circulation is clearly demonstrated for the first time in three-dimensional downscaling simulations

8. conclusions and recommendations

Accurate precipitation downscaling in the Great Plains remains a great challenge for most RCMs, particularly during the warm months [*Liang et al.*, 2006; *F X Qiao and Liang*, 2015; *J L Wang and Kotamarthi*, 2014]. Most previous dynamic downscaling simulations [e.g., *Mearns et al.*, 2012; *X Sun et al.*, 2016] significantly underestimate warm-season precipitation in the region. To improve the results, we conduct in this study WRF simulations with different physics parameterization schemes and nudging strategies, first for a representative warm season, in order to identify an optimal configuration or find a plausible solution to the precipitation bias problem. Results show that different cumulus schemes lead to more pronounced difference in simulated precipitation than other tested physics schemes. Simply altering physics schemes (including cumulus schemes, land surface models, PBL schemes, and microphysics schemes) is not enough to alleviate the dry bias over the southern Great Plains, which appears to be related to an anticyclonic circulation anomaly that develop in the long-term simulations over the central and western parts of the continental U.S. The northerly wind anomaly along the eastern flank of this circulation anomaly decreases the prevailing southerly flows over the Great Plains along the western side of the Bermuda High, advecting less moisture from the Gulf of Mexico to the Great Plains. Thus, the anticyclonic circulation anomaly that develops in the continuous, long-term WRF simulation decreases moisture supply to the southern Great Plains and thereby suppresses its associated precipitation.

Interior spectral nudging emerges as an effective solution to reduce the precipitation bias over the Great Plains in the WRF dynamic downscaling. Spectral nudging ensures that the

synoptic-scale circulations follow those in the driving fields while simultaneously allowing the RCM (i.e., WRF in this study) to develop small-scale dynamics, which is consistent with the objective of dynamic downscaling, i.e., to produce additional small-scale details under coarse-resolution forcing. Applying spectral nudging effectively suppresses the circulation anomaly in WRF downscaling. As a result, the dry bias over the Great Plains is effectively alleviated and the downscaling performance in reproducing observed precipitation is significantly improved.

With the optimized WRF model configuration, downscaling is carried out from NCEP/DOE R2 forcing using WRF for a 36-year period (1980-2015) and compared to corresponding results without spectral nudging. The spatial and temporal distributions of monthly climatological precipitation patterns are captured well in the simulation with spectral nudging. Yearly variation of precipitation amount over the Great Plains is also captured with a correlation of 0.743 with the PRISM precipitation data and, overall, the precipitation amount is only over-produced by 0.055 mm day^{-1} (2.4%). Compared to the downscaling results of NARCCAP WRFG and those reported in Sun et al., 2016), our precipitation downscaling represents a substantial improvement. Even though the testing of the configuration is done for the warm season only, improvements over NARCCAP WRFG are seen throughout the whole year.

The precipitation downscaling can greatly affect down-stream impact models. We studied the impact of precipitation downscaling on the trans-state (Oklahoma and Kansas) Oologah Lake watershed of the Great Plains using the VIC model. Because NARCCAP WRFG significantly underestimates precipitation over the Great Plains, especially for Oklahoma and Kansas, the VIC simulations driven by its output consequently significantly underestimate the streamflow at the watershed outlet during most of the year, as reported previously by *L Qiao et al.* [2014b]. With the improved downscaled precipitation from this study, the simulated monthly streamflow rates show a much better agreement with observations.

We note that the WRF downscaling conducted in this study is at a spatial resolution of 20 km, which is larger than the sizes of individual convective storms that frequently occur in the Great Plains. Thus, this method may not be able to accurately simulate convective weather due to its inability to simulate small-scale extreme events [*Y Gao et al.*, 2012; *Gensini and Mote*, 2014; *Mahoney et al.*, 2013; *Andreas F. Prein et al.*, 2017; *X Sun et al.*, 2016; *C X Zhang et al.*, 2012]. Because of the paramount social and economic impacts these events can cause, higher-resolution dynamical climate downscaling with the ability to capture these small-scale extreme

events is warranted to provide the information needed for key local decision-making at relevant (county-level or smaller) scales, particularly for the Great Plains [*Harding and Snyder*, 2014]. Lessons learned from this study may help produce such meaningful higher-resolution dynamic downscaling in the future. When spectral nudging is applied to convection-allowing simulations, as those reported in Sun et al. (2016), further improvements in reproducing features associated with severe weather are expected.

While spectral nudging can alleviate the model bias in an artificial way, the root cause for the model error (i.e., summertime dry bias) over the Great Plains is not revealed clearly with the simulations conducted in this study with different physics schemes. Though not shown here, other sensitivity simulations are also conducted, including changing land properties, different terrain height, different horizontal resolution, and different domain size. The spurious circulation appears initiated west of Mexico (which subsequently leads to a northerly wind anomaly over the Great Plains) and the spurious circulation is related to temperature bias at certain levels, e.g., ~850 hPa, and 500-650 hPa. However, the cause-and-effect relationship between the temperature biases and the spurious circulation yet remains to be revealed in future studies.

Cumulus schemes appear to be the most critical model component to affect precipitation simulations over the Great Plains with a 20 km grid spacing. The scale–aware cumulus schemes (particularly multi-scale KF) show better performance than their non-scale-aware counterparts in terms of precipitation amount and timing/propagation. Because of the continuous advancement of computation resources, climate and operational NWP simulations are now advancing from convection-parameterization resolution to convection-permitting resolution, in rare cases to convection-resolving resolution that requires sub-kilometer grid spacing [*Kwon and Hong*, 2017]. Even though in some convection-permitting simulations (e.g., at 4 km resolution), cumulus schemes are turned off, scale-aware cumulus schemes appear more appropriate in the gray zone (1-15km), which can bring the convection-parameterization simulations seamlessly converge to convection-resolving simulations as the horizontal grid size is reduced. Also the advantages of scale-aware cumulus schemes over non-scale-aware schemes can be more appreciable in the gray zone. Until cloud-resolving simulations become widely affordable, which may take years, further development/refinement/evaluation of scale-aware cumulus schemes (such as Grell-Freitas and multi-scale KF) to improve simulations at the gray-zone resolution (1-15km) is warranted [*A. Arakawa and Jung*, 2011; *Akio Arakawa et al.*, 2016;

Gerard et al., 2009; *S-Y Hong and Dudhia*, 2012; *Kwon and Hong*, 2017; *Leung and Gao*, 2016].

Based on our analysis of high resolution (4km) WRF downscaling outputs and 14-year (i.e., 2002-2015) Stage IV precipitation data, the role of the Edwards Plateau in modulating August precipitation distribution is investigated. In this month, the total precipitation east of the Balcones Escarpment is suppressed. The precipitation over the eastern part of the Edwards Plateau appears separated from the other precipitation area in the east, south, and west. Locally initiated moist convection in the afternoon contributes most to the total precipitation during this month in the region. The dynamically downscaled simulations nicely capture the spatial patterns of both afternoon precipitation frequency and amount, matching the simulated upward motions. The upward motion does not occur in the region with the largest slope (i.e., western side of the Edwards Plateau); instead, it occurs in some regions with a gentle slope, e.g., east of DFW. Thus, the Mountain-Plains Solenoid (MPS) circulation (which is supposed to be most prominent at places with the largest horizontal elevation differences) cannot explain the dominant vertical motions.

Land surface processes are examined to search for possible explanation for the specific pattern of upward motions over the Edwards Plateau. In fact, the spatial pattern of vertical velocity matches that of surface sensible heat fluxes quite well, which is found to be primarily tied to the soil type. The clay-based soil types dominant over the Edwards Plateau have a relatively higher dry-soil moisture threshold and wilting-point soil moisture than their sandy counterparts dominant over the plain to the east. Thus, clay-based soils can retain more of their soil moisture, reducing evapotranspiration and limiting latent heat fluxes, consequently leading to higher sensible heat fluxes. As a result of high sensible heat flux, vertical motion is induced, helping to trigger afternoon moist convection over the Edwards Plateau under favorable conditions.

9. outreach

Two articles were published out of the work of this project:

Hu, X.-M., M. Xue, R. A. McPherson, E. Martin, D. H. Rosendahl, and L. Qiao (2018), Precipitation dynamical downscaling over the Great Plains, *J. Adv. Modeling Earth Systems*,10.1002/2017MS001154

Hu, X.-M., M. Xue, and R. A. McPherson (2017), The Importance of Soil-Type Contrast in Modulating August Precipitation Distribution near the Edwards Plateau and Balcones Escarpment in Texas, *J. Geophys. Res.*, doi:10.1002/2017JD027035

The produced precipitation downscaling data and some other meteorological data were passed to Lei Qiao (Oklahoma State University) for hydrological assessment using the VIC model.

New proposals to extend beyond this project were submitted to seek further funding for CAPS's dynamic downscaling work.

Reference:

Alapaty, K., J. A. Herwehe, T. L. Otte, C. G. Nolte, O. R. Bullock, M. S. Mallard, J. S. Kain, and J. Dudhia (2012), Introducing subgrid-scale cloud feedbacks to radiation for regional meteorological and climate modeling, Geophys Res Lett, 39(24), L24809, doi: 10.1029/2012GL054031.

Arakawa, A., and J. H. Jung (2011), Multiscale modeling of the moist-convective atmosphere - A review, Atmos Res, 102(3), 263-285.

Arakawa, A., J. H. Jung, and C. M. Wu (2011), Toward unification of the multiscale modeling of the atmosphere, Atmos Chem Phys, 11(8), 3731-3742.

Arakawa, A., J.-H. Jung, and C.-M. Wu (2016), Multiscale Modeling of the Moist-Convective Atmosphere, Meteorological Monographs, 56, 16.11-16.17, doi: 10.1175/amsmonographs-d-15-0014.1.

Argueso, D., J. M. Hidalgo-Munoz, S. R. Gamiz-Fortis, M. J. Esteban-Parra, J. Dudhia, and Y. Castro-Diez (2011), Evaluation of WRF Parameterizations for Climate Studies over Southern Spain Using a Multistep Regionalization, J Climate, 24(21), 5633-5651.

Arritt, R. W., T. D. Rink, M. Segal, D. P. Todey, C. A. Clark, M. J. Mitchell, and K. M. Labas (1997), The great plains low-level jet during the warm season of 1993, Mon Weather Rev, 125(9), 2176-2192.

Baldwin, M. E., J. S. Kain, and M. P. Kay (2002), Properties of the convection scheme in NCEP's eta model that affect forecast sounding interpretation, Weather Forecast, 17(5), 1063-1079.

Bao, X. H., and F. Q. Zhang (2013), Impacts of the mountain-plains solenoid and cold pool dynamics on the diurnal variation of warm-season precipitation over northern China, Atmos Chem Phys, 13(14), 6965-6982, doi: 10.5194/acp-13-6965-2013.

Berg, A., K. Findell, B. R. Lintner, P. Gentine, and C. Kerr (2013), Precipitation Sensitivity to Surface Heat Fluxes over North America in Reanalysis and Model Data, J Hydrometeorol, 14(3), 722-743, doi: 10.1175/Jhm-D-12-0111.1.

Betts, A. K. (1986), A New Convective Adjustment Scheme .1. Observational and Theoretical Basis, Q J Roy Meteor Soc, 112(473), 677-691.

Betts, A. K., and M. J. Miller (1986), A New Convective Adjustment Scheme .2. Single Column Tests Using Gate Wave, Bomex, Atex and Arctic Air-Mass Data Sets, Q J Roy Meteor Soc, 112(473), 693-709.

Betts, A. K., F. Chen, K. E. Mitchell, and Z. I. Janjic (1997), Assessment of the land surface and boundary layer models in two operational versions of the NCEP Eta Model using FIFE data, Monthly Weather Review, 125(11), 2896-2916, doi: Doi 10.1175/1520-0493(1997)125<2896:Aotlsa>2.0.Co;2.

Bryan, G. H., J. C. Wyngaard, and J. M. Fritsch (2003), Resolution requirements for the simulation of deep moist convection, Mon Weather Rev, 131(10), 2394-2416.

Bukovsky, M. S., and D. J. Karoly (2009), Precipitation Simulations Using WRF as a Nested Regional Climate Model, J Appl Meteorol Clim, 48(10), 2152-2159, doi: 10.1175/2009jamc2186.1.
Bukovsky, M. S., J. S. Kain, and M. E. Baldwin (2006), Bowing convective systems in a popular operational model: Are they for real?, Weather Forecast, 21(3), 307-324.
Bullock, O. R. J., K. Alapaty, J. A. Herwehe, and J. S. Kain (2015), A Dynamically Computed Convective Time Scale for the Kain–Fritsch Convective Parameterization Scheme, Mon Weather Rev, 143(6), 2105-2120, doi: 10.1175/mwr-d-14-00251.1.
Carbone, R. E., and J. D. Tuttle (2008), Rainfall occurrence in the US warm season: The diurnal cycle, J Climate, 21(16), 4132-4146.
Chen, F., and J. Dudhia (2001), Coupling an advanced land surface-hydrology model with the Penn State-NCAR MM5 modeling system. Part I: Model implementation and sensitivity, Monthly Weather Review, 129(4), 569-585, doi: Doi 10.1175/1520-0493(2001)129<0569:Caalsh>2.0.Co;2.
Choi, I. J., E. K. Jin, J. Y. Han, S. Y. Kim, and Y. Kwon (2015), Sensitivity of diurnal variation in simulated precipitation during East Asian summer monsoon to cumulus parameterization schemes, J Geophys Res-Atmos, 120(23), doi: 10.1002/2015jd023810.
Chu, W., X. G. Gao, and S. Sorooshian (2011), A Solution to the Crucial Problem of Population Degeneration in High-Dimensional Evolutionary Optimization, Ieee Syst J, 5(3), 362-373, doi: 10.1109/Jsyst.2011.2158682.
Clark, A. J., W. A. Gallus, M. Xue, and F. Y. Kong (2009), A Comparison of Precipitation Forecast Skill between Small Convection-Allowing and Large Convection-Parameterizing Ensembles, Weather Forecast, 24(4), 1121-1140, doi: 10.1175/2009waf2222222.1.
Dai, A., F. Giorgi, and K. E. Trenberth (1999), Observed and model-simulated diurnal cycles of precipitation over the contiguous United States, J Geophys Res-Atmos, 104(D6), 6377-6402, doi: Doi 10.1029/98jd02720.
Daly, C., R. P. Neilson, and D. L. Phillips (1994), A Statistical Topographic Model for Mapping Climatological Precipitation over Mountainous Terrain, J Appl Meteorol, 33(2), 140-158, doi: Doi 10.1175/1520-0450(1994)033<0140:Astmfm>2.0.Co;2.
Denis, B., J. Cote, and R. Laprise (2002), Spectral decomposition of two-dimensional atmospheric fields on limited-area domains using the discrete cosine transform (DCT), Mon Weather Rev, 130(7), 1812-1829, doi: Doi 10.1175/1520-0493(2002)130<1812:Sdotda>2.0.Co;2.
Dudhia, J. (1989), Numerical Study of Convection Observed during the Winter Monsoon Experiment Using a Mesoscale Two-Dimensional Model, J Atmos Sci, 46(20), 3077-3107, doi: Doi 10.1175/1520-0469(1989)046<3077:Nsocod>2.0.Co;2.
European Centre for Medium-Range Weather Forecasts (2009), ERA-Interim Project, edited, Research Data Archive at the National Center for Atmospheric Research, Computational and Information Systems Laboratory, Boulder, CO.
Fast, J. D., and M. D. Mccorcle (1990), A 2-Dimensional Numerical Sensitivity Study of the Great-Plains Low-Level Jet, Monthly Weather Review, 118(1), 151-163, doi: Doi 10.1175/1520-0493(1990)118<0151:Atdnss>2.0.Co;2.
Fast, J. D., and M. D. Mccorcle (1991), The Effect of Heterogeneous Soil-Moisture on a Summer Baroclinic Circulation in the Central United-States, Monthly Weather Review, 119(9), 2140-2167, doi: Doi 10.1175/1520-0493(1991)119<2140:Teohsm>2.0.Co;2.
Findell, K. L., P. Gentine, B. R. Lintner, and C. Kerr (2011), Probability of afternoon precipitation in eastern United States and Mexico enhanced by high evaporation, Nat Geosci, 4(7), 434-439, doi: 10.1038/Ngeo1174.

Flaounas, E., S. Bastin, and S. Janicot (2011), Regional climate modelling of the 2006 West African monsoon: sensitivity to convection and planetary boundary layer parameterisation using WRF, Clim Dynam, 36(5-6), 1083-1105.
Fowler, L. D., W. C. Skamarock, G. A. Grell, S. R. Freitas, and M. G. Duda (2016), Analyzing the Grell-Freitas Convection Scheme from Hydrostatic to Nonhydrostatic Scales within a Global Model, Mon Weather Rev, 144(6), 2285-2306.
Gallus, W. A. (1999), Eta simulations of three extreme precipitation events: Sensitivity to resolution and convective parameterization, Weather Forecast, 14(3), 405-426.
Gao, Y., L. R. Leung, C. Zhao, and S. Hagos (2017), Sensitivity of US summer precipitation to model resolution and convective parameterizations across gray zone resolutions, J Geophys Res-Atmos, 122(5), 2714-2733, doi: 10.1002/2016jd025896.
Gao, Y., J. S. Fu, J. B. Drake, Y. Liu, and J. F. Lamarque (2012), Projected changes of extreme weather events in the eastern United States based on a high resolution climate modeling system, Environ Res Lett, 7(4), doi: 044025, 10.1088/1748-9326/7/4/044025.
Gao, Y. X., M. C. Tang, S. W. Luo, Z. B. Shen, and C. Li (1981), Some Aspects of Recent Research on the Qinghai-Xizang Plateau Meteorology, B Am Meteorol Soc, 62(1), 31-35, doi: Doi 10.1175/1520-0477(1981)062<0031:Saorro>2.0.Co;2.
Gensini, V. A., and T. L. Mote (2014), Estimations of Hazardous Convective Weather in the United States Using Dynamical Downscaling, J Climate, 27(17), 6581-6589, doi: 10.1175/Jcli-D-13-00777.1.
Gerard, L., J. M. Piriou, R. Brozkova, and J. F. Geleyn (2009), Cloud and Precipitation Parameterization in a Meso-Gamma-Scale Operational Weather Prediction Model, Mon Weather Rev, 137(11), 3960-3977.
Gochis, D. J., W. J. A. Shuttleworth, and Z. L. Yang (2002), Sensitivity of the modeled North American monsoon regional climate to convective parameterization, Mon Weather Rev, 130(5), 1282-1298, doi: Doi 10.1175/1520-0493(2002)130<1282:Sotmna>2.0.Co;2.
Gochis, D. J., W. J. Shuttleworth, and Z. L. Yang (2003), Hydrometeorological response of the modeled North American monsoon to convective parameterization, J Hydrometeorol, 4(2), 235-250, doi: Doi 10.1175/1525-7541(2003)4<235:Hrotmn>2.0.Co;2.
Gomez, B., and G. Miguez-Macho (2017), The impact of wave number selection and spin-up time in spectral nudging, Q J Roy Meteor Soc, 143(705), 1772-1786, doi: 10.1002/qj.3032.
Grell, G. A., and D. Devenyi (2002), A generalized approach to parameterizing convection combining ensemble and data assimilation techniques, Geophys Res Lett, 29(14), doi: 1693, 10.1029/2002gl015311.
Grell, G. A., and S. R. Freitas (2014), A scale and aerosol aware stochastic convective parameterization for weather and air quality modeling, Atmos Chem Phys, 14(10), 5233-5250, doi: 10.5194/acp-14-5233-2014.
Harding, K. J., and P. K. Snyder (2014), Examining future changes in the character of Central U.S. warm-season precipitation using dynamical downscaling, J Geophys Res-Atmos, 119(23), 13116-13136.
Harding, K. J., P. K. Snyder, and S. Liess (2013), Use of dynamical downscaling to improve the simulation of Central US warm season precipitation in CMIP5 models, J Geophys Res-Atmos, 118(22), 12522-12536.
Harris, L. M., and S. J. Lin (2014), Global-to-Regional Nested Grid Climate Simulations in the GFDL High Resolution Atmospheric Model, J Climate, 27(13), 4890-4910, doi: 10.1175/Jcli-D-13-00596.1.
He, H. Z., and F. Q. Zhang (2010), Diurnal Variations of Warm-Season Precipitation over Northern China, Monthly Weather Review, 138(4), 1017-1025, doi: 10.1175/2010mwr3356.1.

Helfand, H. M., and S. D. Schubert (1995), Climatology of the Simulated Great-Plains Low-Level Jet and Its Contribution to the Continental Moisture Budget of the United-States, J Climate, 8(4), 784-806.
Herman, G. R., and R. S. Schumacher (2016), Extreme Precipitation in Models: An Evaluation, Weather Forecast, 31(6), 1853-1879, doi: 10.1175/waf-d-16-0093.1.
Herwehe, J. A., K. Alapaty, T. L. Spero, and C. G. Nolte (2014), Increasing the credibility of regional climate simulations by introducing subgrid-scale cloud-radiation interactions, J Geophys Res-Atmos, 119(9), 5317-5330.
Higgins, R. W., Y. Yao, E. S. Yarosh, J. E. Janowiak, and K. C. Mo (1997), Influence of the Great Plains low-level jet on summertime precipitation and moisture transport over the central United States, J Climate, 10(3), 481-507.
Hong, S.-Y., and J. Dudhia (2012), Next-Generation Numerical Weather Prediction: Bridging Parameterization, Explicit Clouds, and Large Eddies, B Am Meteorol Soc, 93(1), ES6-ES9, doi: 10.1175/2011bams3224.1.
Hong, S. Y., Y. Noh, and J. Dudhia (2006), A new vertical diffusion package with an explicit treatment of entrainment processes, Mon Weather Rev, 134(9), 2318-2341, doi: Doi 10.1175/Mwr3199.1.
Hu, X.-M., and M. Xue (2016), Influence of Synoptic Sea-Breeze Fronts on the Urban Heat Island Intensity in Dallas–Fort Worth, Texas, Monthly Weather Review, 144(4), 1487-1507, doi: 10.1175/mwr-d-15-0201.1.
Hu, X.-M., F. Q. Zhang, and J. W. Nielsen-Gammon (2010), Ensemble-based simultaneous state and parameter estimation for treatment of mesoscale model error: A real-data study, Geophys Res Lett, 37, doi: L08802, 10.1029/2010gl043017.
Hu, X.-M., J. W. Nielsen-Gammon, and F. Q. Zhang (2010), Evaluation of Three Planetary Boundary Layer Schemes in the WRF Model, J Appl Meteorol Clim, 49(9), 1831-1844, doi: 10.1175/2010jamc2432.1.
Hu, X.-M., P. M. Klein, and M. Xue (2013), Evaluation of the updated YSU planetary boundary layer scheme within WRF for wind resource and air quality assessments, J Geophys Res-Atmos, 118(18), 10490-10505, doi: 10.1002/jgrd.50823.
Hu, X.-M., M. Xue, and R. A. McPherson (2017), The Importance of Soil Type Contrast in Modulating August Precipitation Distribution near the Edwards Plateau and Balcones Escarpment in Texas, J. Geophys. Res., doi: 10.1002/2017JD027035
Hu, X.-M., D. C. Doughty, K. J. Sanchez, E. Joseph, and J. D. Fuentes (2012), Ozone variability in the atmospheric boundary layer in Maryland and its implications for vertical transport model, Atmos Environ, 46, 354-364, doi: DOI 10.1016/j.atmosenv.2011.09.054.
Hu, X.-M., Z. Q. Ma, W. L. Lin, H. L. Zhang, J. L. Hu, Y. Wang, X. B. Xu, J. D. Fuentes, and M. Xue (2014), Impact of the Loess Plateau on the atmospheric boundary layer structure and air quality in the North China Plain: A case study, Sci Total Environ, 499, 228-237, doi: DOI 10.1016/j.scitotenv.2014.08.053.
Huang, W.-R., Y.-H. Chang, H.-H. Hsu, C.-T. Cheng, and C.-Y. Tu (2016), Dynamical downscaling simulation and future projection of summer rainfall in Taiwan: Contributions from different types of rain events, Journal of Geophysical Research: Atmospheres, 121(23), 13,973-913,988, doi: 10.1002/2016JD025643.
Janjic, Z. I. (1994), The Step-Mountain Eta Coordinate Model - Further Developments of the Convection, Viscous Sublayer, and Turbulence Closure Schemes, Mon Weather Rev, 122(5), 927-945, doi: Doi 10.1175/1520-0493(1994)122<0927:Tsmecm>2.0.Co;2.

Jankov, I., W. A. Gallus, M. Segal, B. Shaw, and S. E. Koch (2005), The impact of different WRF model physical parameterizations and their interactions on warm season MCS rainfall, Weather Forecast, 20(6), 1048-1060, doi: Doi 10.1175/Waf888.1.
Kain, J. S. (2004), The Kain-Fritsch convective parameterization: An update, J Appl Meteorol, 43(1), 170-181, doi: Doi 10.1175/1520-0450(2004)043<0170:Tkcpau>2.0.Co;2.
Kanamitsu, M., W. Ebisuzaki, J. Woollen, S. K. Yang, J. J. Hnilo, M. Fiorino, and G. L. Potter (2002), NCEP-DOE AMIP-II reanalysis (R-2), B Am Meteorol Soc, 83(11), 1631-1643, doi: 10.1175/Bams-83-11-1631.
Kang, S.-L. (2016), Regional Bowen ratio controls on afternoon moist convection: A large eddy simulation study, Journal of Geophysical Research: Atmospheres, n/a-n/a, doi: 10.1002/2016JD025567.
Klein, C., D. Heinzeller, J. Bliefernicht, and H. Kunstmann (2015), Variability of West African monsoon patterns generated by a WRF multi-physics ensemble, Clim Dynam, 45(9-10), 2733-2755, doi: 10.1007/s00382-015-2505-5.
Klein, P. M., X.-M. Hu, A. Shapiro, and M. Xue (2016), Linkages Between Boundary-Layer Structure and the Development of Nocturnal Low-Level Jets in Central Oklahoma, Bound-Lay Meteorol, 158(3), 383-408, doi: 10.1007/s10546-015-0097-6.
Klein, S. A., X. N. Jiang, J. Boyle, S. Malyshev, and S. C. Xie (2006), Diagnosis of the summertime warm and dry bias over the U.S. Southern Great Plains in the GFDL climate model using a weather forecasting approach, Geophys Res Lett, 33(18), doi: L18805, 10.1029/2006gl027567.
Kong, F., M. Xue, K. W. Thomas, and (2011), CAPS storm-scale ensemble forecasts in NOAA HWT 2011 Spring Experiment: Sensitivities of WRF model physics, in *12th Annual WRF Users' Workshop*, edited, p. 6.3, Amer. Meteor. Soc., Boulder, CO.
Kwon, Y. C., and S. Y. Hong (2017), A Mass-Flux Cumulus Parameterization Scheme across Gray-Zone Resolutions, Mon Weather Rev, 145(2), 583-598.
Lee, H., D. E. Waliser, R. Ferraro, T. Iguchi, C. D. Peters-Lidard, B. Tian, P. C. Loikith, and D. B. Wright (2017), Evaluating hourly rainfall characteristics over the U.S. Great Plains in dynamically downscaled climate model simulations using NASA-Unified WRF, Journal of Geophysical Research: Atmospheres, 122(14), 7371-7384, doi: 10.1002/2017jd026564.
Lee, M. I., S. D. Schubert, M. J. Suarez, J. K. E. Schemm, H. L. Pan, J. Han, and S. H. Yoo (2008), Role of convection triggers in the simulation of the diurnal cycle of precipitation over the United States Great Plains in a general circulation model, J Geophys Res-Atmos, 113(D2), doi: D02111, 10.1029/2007jd008984.
Lee, M. I., S. D. Schubert, M. J. Suarez, I. M. Held, N. C. Lau, J. J. Ploshay, A. Kumar, H. K. Kim, and J. K. E. Schemm (2007a), An analysis of the warm-season diurnal cycle over the continental united states and northern Mexico in general circulation models, J Hydrometeorol, 8(3), 344-366.
Lee, M. I., et al. (2007b), Sensitivity to horizontal resolution in the AGCM simulations of warm season diurnal cycle of precipitation over the United States and northern Mexico, J Climate, 20(9), 1862-1881, doi: https://doi.org/10.1175/JCLI4090.1.
Leung, L. R., and Y. Gao (2016), Regional downscaling of S2S prediction: Past lessons and future prospects, CLIVAR Var., 14(4), 13–17.
Leung, L. R., Y. H. Kuo, and J. Tribbia (2006), Research needs and directions of regional climate modeling using WRF and CCSM, B Am Meteorol Soc, 87(12), 1747-1751, doi: 10.1175/Bams-887-12-1747.

Liang, X. Z., L. Li, A. Dai, and K. E. Kunkel (2004), Regional climate model simulation of summer precipitation diurnal cycle over the United States, Geophys Res Lett, 31(24), doi: L24208, 10.1029/2004gl021054.
Liang, X. Z., J. P. Pan, J. H. Zhu, K. E. Kunkel, J. X. L. Wang, and A. Dai (2006), Regional climate model downscaling of the U.S. summer climate and future change, J Geophys Res-Atmos, 111(D10), doi: D10108, 10.1029/2005jd006685.
Lim, K. S. S., S. Y. Hong, J. H. Yoon, and J. Han (2014), Simulation of the Summer Monsoon Rainfall over East Asia Using the NCEP GFS Cumulus Parameterization at Different Horizontal Resolutions, Weather Forecast, 29(5), 1143-1154.
Lin, Y. (2011), GCIP/EOP Surface: Precipitation NCEP/EMC 4KM Gridded Data (GRIB) Stage IV Data, edited by U. N.-E. O. Laboratory, UCAR/NCAR - Earth Observing Laboratory.
Liu, P., A. P. Tsimpidi, Y. Hu, B. Stone, A. G. Russell, and A. Nenes (2012), Differences between downscaling with spectral and grid nudging using WRF, Atmos Chem Phys, 12(8), 3601-3610, doi: 10.5194/acp-12-3601-2012.
Liu, S., Y. Wei, W. M. Post, R. B. Cook, K. Schaefer, and M. M. Thornton (2013), The Unified North American Soil Map and its implication on the soil organic carbon stock in North America, Biogeosciences, 10(5), 2915-2930, doi: 10.5194/bg-10-2915-2013.
Liu, X. D., A. J. Bai, and C. H. Liu (2009), Diurnal variations of summertime precipitation over the Tibetan Plateau in relation to orographically-induced regional circulations, Environ Res Lett, 4(4), doi: 045203, 10.1088/1748-9326/4/4/045203.
Lo, J. C. F., Z. L. Yang, and R. A. Pielke (2008), Assessment of three dynamical climate downscaling methods using the Weather Research and Forecasting (WRF) model, J Geophys Res-Atmos, 113(D9), doi: D09112, 10.1029/2007jd009216.
Lynn, B. H., R. Healy, and L. M. Druyan (2009), Quantifying the sensitivity of simulated climate change to model configuration, Climatic Change, 92(3-4), 275-298.
Ma, H. Y., et al. (2014), On the Correspondence between Mean Forecast Errors and Climate Errors in CMIP5 Models, J Climate, 27(4), 1781-1798, doi: 10.1175/Jcli-D-13-00474.1.
Mabuchi, K., Y. Sato, and H. Kida (2002), Verification of the climatic features of a regional climate model with BAIM, J Meteorol Soc Jpn, 80(4), 621-644, doi: DOI 10.2151/jmsj.80.621.
Mahfouf, J. F., E. Richard, and P. Mascart (1987), The Influence of Soil and Vegetation on the Development of Mesoscale Circulations, J Clim Appl Meteorol, 26(11), 1483-1495, doi: Doi 10.1175/1520-0450(1987)026<1483:Tiosav>2.0.Co;2.
Mahoney, K., M. Alexander, J. D. Scott, and J. Barsugli (2013), High-Resolution Downscaled Simulations of Warm-Season Extreme Precipitation Events in the Colorado Front Range under Past and Future Climates, J Climate, 26(21), 8671-8689.
Martynov, A., R. Laprise, L. Sushama, K. Winger, L. Separovic, and B. Dugas (2013), Reanalysis-driven climate simulation over CORDEX North America domain using the Canadian Regional Climate Model, version 5: model performance evaluation, Clim Dynam, 41(11-12), 2973-3005, doi: 10.1007/s00382-013-1778-9.
Maurer, E. P., A. W. Wood, J. C. Adam, D. P. Lettenmaier, and B. Nijssen (2002), A long-term hydrologically based dataset of land surface fluxes and states for the conterminous United States, J Climate, 15(22), 3237-3251, doi: Doi 10.1175/1520-0442(2002)015<3237:Althbd>2.0.Co;2.
Mearns, L. O., et al. (2012), THE NORTH AMERICAN REGIONAL CLIMATE CHANGE ASSESSMENT PROGRAM Overview of Phase I Results, B Am Meteorol Soc, 93(9), 1337-1362.
Mesinger, F., et al. (2006), North American regional reanalysis, B Am Meteorol Soc, 87(3), 343-360, doi: 10.1175/Bams-87-3-343.

Michelson, S. A., and J. W. Bao (2008), Sensitivity of Low-Level Winds Simulated by the WRF Model in California's Central Valley to Uncertainties in the Large-Scale Forcing and Soil Initialization, J Appl Meteorol Clim, 47(12), 3131-3149, doi: 10.1175/2008jamc1782.1.
Miguez-Macho, G., G. L. Stenchikov, and A. Robock (2004), Spectral nudging to eliminate the effects of domain position and geometry in regional climate model simulations, J Geophys Res-Atmos, 109(D13), doi: D13104, 10.1029/2003jd004495.
Miguez-Macho, G., G. L. Stenchikov, and A. Robock (2005), Regional climate simulations over North America: Interaction of local processes with improved large-scale flow, J Climate, 18(8), 1227-1246, doi: Doi 10.1175/Jcli3369.1.
Mlawer, E. J., S. J. Taubman, P. D. Brown, M. J. Iacono, and S. A. Clough (1997), Radiative transfer for inhomogeneous atmospheres: RRTM, a validated correlated-k model for the longwave, J Geophys Res-Atmos, 102(D14), 16663-16682, doi: Doi 10.1029/97jd00237.
Morrison, H., G. Thompson, and V. Tatarskii (2009), Impact of Cloud Microphysics on the Development of Trailing Stratiform Precipitation in a Simulated Squall Line: Comparison of One- and Two-Moment Schemes, Monthly Weather Review, 137(3), 991-1007, doi: 10.1175/2008mwr2556.1.
National Centers for Environmental Prediction National Weather Service Noaa U. S. Department of Commerce (2000), NCEP/DOE Reanalysis 2 (R2), edited, Research Data Archive at the National Center for Atmospheric Research, Computational and Information Systems Laboratory, Boulder, CO.
National Centers for Environmental Prediction National Weather Service Noaa U. S. Department of Commerce (2005), NCEP North American Regional Reanalysis (NARR), edited, Research Data Archive at the National Center for Atmospheric Research, Computational and Information Systems Laboratory, Boulder, CO.
Nelson, B. R., O. P. Prat, D. J. Seo, and E. Habib (2016), Assessment and Implications of NCEP Stage IV Quantitative Precipitation Estimates for Product Intercomparisons, Weather Forecast, 31(2), 371-394, doi: 10.1175/Waf-D-14-00112.1.
Nielsen-Gammon, J. W., X. M. Hu, F. Q. Zhang, and J. E. Pleim (2010), Evaluation of Planetary Boundary Layer Scheme Sensitivities for the Purpose of Parameter Estimation, Mon Weather Rev, 138(9), 3400-3417, doi: 10.1175/2010mwr3292.1.
Nordeng, T. E. (1995), Extended versions of the convective parameterization scheme at ECMWF and their impact on the mean and transient activity of the model in the Tropics*Rep. ECMWF Research Department Tech. Memo. 206*, 41 pp.
Otte, T. L., C. G. Nolte, M. J. Otte, and J. H. Bowden (2012), Does Nudging Squelch the Extremes in Regional Climate Modeling?, J Climate, 25(20), 7046-7066, doi: 10.1175/Jcli-D-12-00048.1.
Paul, S., S. Ghosh, R. Oglesby, A. Pathak, A. Chandrasekharan, and R. A. A. J. Ramsankaran (2016), Weakening of Indian Summer Monsoon Rainfall due to Changes in Land Use Land Cover, Sci Rep-Uk, 6, doi: 32177, 10.1038/srep32177.
Pieri, A. B., J. von Hardenberg, A. Parodi, and A. Provenzale (2015), Sensitivity of Precipitation Statistics to Resolution, Microphysics, and Convective Parameterization: A Case Study with the High-Resolution WRF Climate Model over Europe, J Hydrometeorol, 16(4), 1857-1872.
Prat, O. P., and B. R. Nelson (2015), Evaluation of precipitation estimates over CONUS derived from satellite, radar, and rain gauge data sets at daily to annual scales (2002-2012), Hydrol Earth Syst Sc, 19(4), 2037-2056, doi: 10.5194/hess-19-2037-2015.
Prein, A. F., R. M. Rasmussen, K. Ikeda, C. Liu, M. P. Clark, and G. J. Holland (2017), The future intensification of hourly precipitation extremes, Nature Clim. Change, 7(1), 48-52, doi:

10.1038/nclimate3168, http://www.nature.com/nclimate/journal/v7/n1/abs/nclimate3168.html - supplementary-information.
Prein, A. F., et al. (2015), A review on regional convection-permitting climate modeling: Demonstrations, prospects, and challenges, Rev Geophys, 53(2), 323-361.
Qiao, F. X., and X. Z. Liang (2015), Effects of cumulus parameterizations on predictions of summer flood in the Central United States, Clim Dynam, 45(3-4), 727-744, doi: 10.1007/s00382-014-2301-7.
Qiao, L., C. B. Zou, C. F. Gaitán, Y. Hong, and R. A. McPherson (2017), Analysis of precipitation projections over the climate gradient of the Arkansas-Red River Basin, J Appl Meteorol Clim, 0(0), null, doi: 10.1175/jamc-d-16-0201.1.
Qiao, L., Y. Hong, S. Chen, C. B. Zou, J. J. Gourley, and B. Yong (2014a), Performance assessment of the successive Version 6 and Version 7 TMPA products over the climate-transitional zone in the southern Great Plains, USA, J Hydrol, 513, 446-456, doi: 10.1016/j.jhydrol.2014.03.040.
Qiao, L., Y. Hong, R. McPherson, M. Shafer, D. Gade, D. Williams, S. Chen, and D. Lilly (2014b), Climate Change and Hydrological Response in the Trans-State Oologah Lake Watershed-Evaluating Dynamically Downscaled NARCCAP and Statistically Downscaled CMIP3 Simulations with VIC Model, Water Resour Manag, 28(10), 3291-3305, doi: 10.1007/s11269-014-0678-z.
Ramsey, N. R., P. M. Klein, and B. Moore (2014), The impact of meteorological parameters on urban air quality, Atmos Environ, 86, 58-67, doi: 10.1016/j.atmosenv.2013.12.006.
Schumacher, R. S., A. J. Clark, M. Xue, and F. Y. Kong (2013), Factors Influencing the Development and Maintenance of Nocturnal Heavy-Rain-Producing Convective Systems in a Storm-Scale Ensemble, Mon Weather Rev, 141(8), 2778-2801, doi: 10.1175/Mwr-D-12-00239.1.
Shin, H. H., and S. Y. Hong (2015), Representation of the Subgrid-Scale Turbulent Transport in Convective Boundary Layers at Gray-Zone Resolutions, Mon Weather Rev, 143(1), 250-271, doi: 10.1175/Mwr-D-14-00116.1.
Sikder, S., and F. Hossain (2016), Assessment of the weather research and forecasting model generalized parameterization schemes for advancement of precipitation forecasting in monsoon-driven river basins, Journal of Advances in Modeling Earth Systems, 8(3), 1210-1228.
Spero, T. L., M. J. Otte, J. H. Bowden, and C. G. Nolte (2014), Improving the representation of clouds, radiation, and precipitation using spectral nudging in the Weather Research and Forecasting model, J Geophys Res-Atmos, 119(20), 11682-11694, doi: 10.1002/2014jd022173.
Sun, J. H., and F. Q. Zhang (2012), Impacts of Mountain-Plains Solenoid on Diurnal Variations of Rainfalls along the Mei-Yu Front over the East China Plains, Monthly Weather Review, 140(2), 379-397, doi: 10.1175/Mwr-D-11-00041.1.
Sun, X., M. Xue, J. Brotzge, R. A. McPherson, X.-M. Hu, and X.-Q. Yang (2016), An evaluation of dynamical downscaling of Central Plains summer precipitation using a WRF-based regional climate model at a convection-permitting 4 km resolution, Journal of Geophysical Research: Atmospheres, 121(23), 13,801-813,825, doi: 10.1002/2016JD024796.
Surcel, M., I. Zawadzki, and M. K. Yau (2014), On the Filtering Properties of Ensemble Averaging for Storm-Scale Precipitation Forecasts, Mon Weather Rev, 142(3), 1093-1105, doi: 10.1175/Mwr-D-13-00134.1.
Tang, Y., S. Y. Zhong, J. A. Winker, and C. K. Walters (2016), Evaluation of the southerly low-level jet climatology for the central United States as simulated by NARCCAP regional climate models, Int J Climatol, 36(13), 4338-4357, doi: 10.1002/joc.4636.

Taylor, C. M., R. A. M. de Jeu, F. Guichard, P. P. Harris, and W. A. Dorigo (2012), Afternoon rain more likely over drier soils, Nature, 489(7416), 423-426, doi: 10.1038/nature11377.
Tian, B., et al. (2017), Development of a Model Performance Metric and Its Application to Assess Summer Precipitation over the U.S. Great Plains in Downscaled Climate Simulations, J Hydrometeorol, 18(10), 2781-2799, doi: 10.1175/jhm-d-17-0045.1.
Trier, S. B., M. A. LeMone, F. Chen, and K. W. Manning (2011), Effects of Surface Heat and Moisture Exchange on ARW-WRF Warm-Season Precipitation Forecasts over the Central United States, Weather Forecast, 26(1), 3-25, doi: 10.1175/2010waf2222426.1.
Trier, S. B., F. Chen, K. W. Manning, M. A. LeMone, and C. A. Davis (2008), Sensitivity of the PBL and precipitation in 12-day simulations of warm-season convection using different land surface models and soil wetness conditions, Mon Weather Rev, 136(7), 2321-2343, doi: 10.1175/2007mwr2289.1.
Tripathi, O. P., and F. Dominguez (2013), Effects of spatial resolution in the simulation of daily and subdaily precipitation in the southwestern US, J Geophys Res-Atmos, 118(14), 7591-7605, doi: 10.1002/jgrd.50590.
Tripoli, G. J., and W. R. Cotton (1989a), Numerical Study of an Observed Orogenic Mesoscale Convective System .1. Simulated Genesis and Comparison with Observations, Monthly Weather Review, 117(2), 273-304, doi: Doi 10.1175/1520-0493(1989)117<0273:Nsoaoo>2.0.Co;2.
Tripoli, G. J., and W. R. Cotton (1989b), Numerical Study of an Observed Orogenic Mesoscale Convective System .2. Analysis of Governing Dynamics, Monthly Weather Review, 117(2), 305-328, doi: Doi 10.1175/1520-0493(1989)117<0305:Nsoaoo>2.0.Co;2.
Vincent, C. L., and A. N. Hahmann (2015), The Impact of Grid and Spectral Nudging on the Variance of the Near-Surface Wind Speed, J Appl Meteorol Clim, 54(5), 1021-1038, doi: 10.1175/Jamc-D-14-0047.1.
von Storch, H., H. Langenberg, and F. Feser (2000), A spectral nudging technique for dynamical downscaling purposes, Mon Weather Rev, 128(10), 3664-3673, doi: Doi 10.1175/1520-0493(2000)128<3664:Asntfd>2.0.Co;2.
Wang, J. L., and V. R. Kotamarthi (2013), Assessment of Dynamical Downscaling in Near-Surface Fields with Different Spectral Nudging Approaches Using the Nested Regional Climate Model (NRCM), J Appl Meteorol Clim, 52(7), 1576-1591, doi: 10.1175/Jamc-D-12-0302.1.
Wang, J. L., and V. R. Kotamarthi (2014), Downscaling with a nested regional climate model in near-surface fields over the contiguous United States, J Geophys Res-Atmos, 119(14), 8778-8797, doi: 10.1002/2014jd021696.
Wang, Q. W., M. Xue, and Z. M. Tan (2016), Convective initiation by topographically induced convergence forcing over the Dabie Mountains on 24 June 2010, Adv Atmos Sci, 33(10), 1120-1136, doi: 10.1007/s00376-016-6024-z.
Wang, Y. C., H. L. Pan, and H. H. Hsu (2015), Impacts of the triggering function of cumulus parameterization on warm-season diurnal rainfall cycles at the Atmospheric Radiation Measurement Southern Great Plains site, J Geophys Res-Atmos, 120(20), doi: 10.1002/2015jd023337.
Wi, S., F. Dominguez, M. Durcik, J. Valdes, H. F. Diaz, and C. L. Castro (2012), Climate change projection of snowfall in the Colorado River Basin using dynamical downscaling, Water Resour Res, 48, doi: W05504, 10.1029/2011wr010674.
Wolyn, P. G., and T. B. Mckee (1994), The Mountain Plains Circulation East of a 2-Km-High North South Barrier, Monthly Weather Review, 122(7), 1490-1508, doi: Doi 10.1175/1520-0493(1994)122<1490:Tmpceo>2.0.Co;2.
Wyngaard, J. C. (2004), Toward numerical modeling in the "terra incognita", J Atmos Sci, 61(14), 1816-1826.

Xie, S. C., and M. H. Zhang (2000), Impact of the convection triggering function on single-column model simulations, J Geophys Res-Atmos, 105(D11), 14983-14996.
Xue, M., et al. (2007), CAPS realtime storm-scale ensemble and high-resolution forecasts as part of the NOAA hazardous weather testbed 2007 spring experiment, in *22nd Conf. Wea. Anal. Forecasting/18th Conf. Num. Wea. Pred.*, edited, Amer. Meteor. Soc., Salt Lake City, Utah.
Xue, M., et al. (2009), CAPS realtime multi-model convection-allowing ensemble and 1-km convection-resolving forecasts for the NOAA Hazardous Weather Testbed 2009 Spring Experiement, in *23rd Conf. Wea. Anal. Forecasting/19th Conf. Num. Wea. Pred.*, edited, p. Paper 16, Amer. Meteor. Soc., Omaha, NB.
Xue, M., et al. (2010), CAPS Realtime Storm Scale Ensemble and High Resolution Forecasts for the NOAA Hazardous Weather Testbed 2010 Spring Experiment, in *24th Conf. Wea. Forecasting/20th Conf. Num. Wea. Pred.*, edited, p. 7B.3 Amer. Meteor. Soc., Denver, CO.
Zhang, C. X., Y. Q. Wang, and K. Hamilton (2011), Improved Representation of Boundary Layer Clouds over the Southeast Pacific in ARW-WRF Using a Modified Tiedtke Cumulus Parameterization Scheme, Mon Weather Rev, 139(11), 3489-3513.
Zhang, C. X., Y. Q. Wang, A. Lauer, and K. Hamilton (2012), Configuration and Evaluation of the WRF Model for the Study of Hawaiian Regional Climate, Mon Weather Rev, 140(10), 3259-3277.
Zhang, G. J. (2002), Convective quasi-equilibrium in midlatitude continental environment and its effect on convective parameterization, J Geophys Res-Atmos, 107(D14), doi: 4220, 10.1029/2001jd001005.
Zhang, G. J. (2003), Roles of tropospheric and boundary layer forcing in the diurnal cycle of convection in the U.S. southern great plains, Geophys Res Lett, 30(24), doi: 2281, 10.1029/2003gl018554.
Zhang, Y. C., J. H. Sun, and S. M. Fu (2014), Impacts of diurnal variation of mountain-plain solenoid circulations on precipitation and vortices east of the Tibetan Plateau during the mei-yu season, Adv Atmos Sci, 31(1), 139-153, doi: 10.1007/s00376-013-2052-0.
Zhang, Y. X., V. Duliere, P. W. Mote, and E. P. Salathe (2009), Evaluation of WRF and HadRM Mesoscale Climate Simulations over the US Pacific Northwest, J Climate, 22(20), 5511-5526, doi: 10.1175/2009jcli2875.1.
Zheng, Y., K. Alapaty, J. A. Herwehe, A. D. Del Genio, and D. Niyogi (2016), Improving High-Resolution Weather Forecasts Using the Weather Research and Forecasting (WRF) Model with an Updated Kain-Fritsch Scheme, Mon Weather Rev, 144(3), 833-860, doi: 10.1175/Mwr-D-15-0005.1.
Zhou, B., M. Xue, and K. Zhu (2017), A Grid-Refinement-Based Approach for Modeling the Convective Boundary Layer in the Gray Zone: A Pilot Study, J Atmos Sci, 74(11), 3497-3513, doi: 10.1175/jas-d-16-0376.1.